Identifying eolian dust in the geological record

Meijer, Niels; Dupont-Nivet, Guillaume; Licht, Alexis; Trabucho-Alexandre, João ; Bourquin, Sylvie; Abels, Hemmo A.

DOI
10.1016/j.earscirev.2020.103410

Publication date
2020

Document Version
Final published version

Published in
Earth-Science Reviews

Citation (APA)
Meijer, N., Dupont-Nivet, G., Licht, A., Trabucho-Alexandre, J., Bourquin, S., & Abels, H. A. (2020). Identifying eolian dust in the geological record. *Earth-Science Reviews*, *211*, 1-17. Article 103410. https://doi.org/10.1016/j.earscirev.2020.103410

Earth-Science Reviews 211 (2020) 103410

Contents lists available at ScienceDirect

Earth-Science Reviews

journal homepage: www.elsevier.com/locate/earscirev

Identifying eolian dust in the geological record

Niels Meijer [a,*], Guillaume Dupont-Nivet [a,b,c], Alexis Licht [d], João Trabucho-Alexandre [e], Sylvie Bourquin [b], Hemmo A. Abels [f]

[a] Institute for Geosciences, Universität Potsdam, 14476 Potsdam, Germany
[b] Univ Rennes, CNRS, Géosciences Rennes - UMR CNRS 6118, F-35000 Rennes, France
[c] Key Laboratory of Orogenic Belts and Crustal Evolution, Ministry of Education, School of Earth and Space Sciences, Peking University, Beijing 100871, China
[d] Department of Earth and Space Sciences, University of Washington, Seattle, WA 98195, USA
[e] Department of Earth Sciences, Universiteit Utrecht, P.O. Box 80115, 3508 TC Utrecht, the Netherlands
[f] Department of Geosciences and Engineering, Delft University of Technology, 2628 CN Delft, the Netherlands

ARTICLE INFO

Keywords:
Mineral dust
Loess
Loessite

ABSTRACT

Recognition of terrestrial dust in geological records is essential for reconstructing paleoenvironments and quantifying dust fluxes in the past. However, in contrast to eolian sands, silt-sized dust is difficult to recognize in pre-Quaternary records due to a lack of macroscopic features indicating eolian transport and mixing with alluvial sediments. Windblown dust deposits are commonly identified by comparing their sedimentological and petrological features with Quaternary examples of dust known as loess. Here, we review the characteristics of terrestrial dust deposits and conclude that most of these features are not exclusively windblown and may be formed by alluvial deposits as well. We therefore synthesize a set of criteria which enable a reliable identification and quantification of dust while acknowledging potential contributions of alluvial components. These methods include quartz-grain surface morphology analysis to distinguish eolian and alluvial transport modes, provenance studies to identify local and extrabasinal sources, grain-size-shape end-member modelling to quantify the various sedimentary contributions to the record, and a basin-scale stratigraphic approach to derive regional patterns and avoid interpretation of local phenomena. We reassess the Eocene to Pliocene records of the Chinese Loess Plateau and conclude that these strata represent both alluvial and eolian sediments deposited in extensive mudflat systems. Quaternary loess, by contrast, is almost exclusively composed of windblown dust. The early Pleistocene shift from mudflat to loess deposits is associated with a significant increase in accumulation rates, likely due to increased dust production upwind, overwhelming and blanketing the local mudflat systems in central China.

1. Introduction

Mineral dust is a fundamental component of the Earth system by driving various physical, chemical and biological processes including radiation scattering, cloud nucleation and ocean fertilization (e.g. An et al., 2014; Jickells et al., 2005; Knippertz and Stuut, 2014; Pye, 1987). Geological records of mineral dust enable the reconstruction of dust fluxes in the past and are therefore key to assess its impact on the Earth system. Furthermore, dust deposits provide valuable clues on paleoenvironmental settings such as continental aridity, glacial conditions and dominant wind directions (e.g. An et al., 2014; Soreghan et al., 2002, 2014; Soreghan et al., 2008) and may provide analogues for desertification due to the ongoing global warming (e.g. D'Odorico et al., 2013). However, these studies are all limited by the reliability of recognizing and quantifying windblown dust in the geological record. As a result, the role of dust forcing remains poorly understood and constitutes one of the largest uncertainties in climate model simulations (Heavens et al., 2012; Lee et al., 2016; Schwartz and Andreae, 1996).

Dust is atmospherically transported in suspension and generally contains particles not bigger than ~100 μm (Pye, 1987; Újvári et al., 2016). After settling, these particles form structureless deposits with no sedimentary features diagnostic of eolian transport. This is in contrast to coarser-grained eolian sediments that may form dune cross-bedding and wind ripple laminations after deposition by wind or ventifacts indicating eolian transport (e.g. Hunter, 1977; Durand and Bourquin, 2013). The lack of diagnostic eolian features in silt complicates recognizing dust deposits, especially in pre-Quaternary records where paleowind directions are unknown and geographic relationships between the source

* Corresponding author.
E-mail address: niels.meijer@senckenberg.de (N. Meijer).

https://doi.org/10.1016/j.earscirev.2020.103410
Received 23 July 2020; Received in revised form 12 October 2020; Accepted 14 October 2020
Available online 17 October 2020

and dust bodies are difficult to assess. Yet pre-Quaternary dust has been identified in various records (Fig. 1) including Precambrian siltstones in northern Norway and Svalbard (Edwards, 1979), Triassic mudrocks in England and the North Sea (Jefferson et al., 2002; Wilkins et al., 2018; Wilson et al., 2020), Cenozoic siltstones in Argentina (Bellosi, 2010; Selkin et al., 2015), both Paleozoic and Cenozoic siltstones in western North America (Johnson, 1989; Soreghan et al., 2008; Fan et al., 2020), as well as Permian, Cretaceous and Cenozoic deposits in Central Asia (Carrapa et al., 2015; Chen et al., 2019; Obrist-Farner and Yang, 2016; Sun and Windley, 2015; Wasiljeff et al., 2020).

To overcome the lack of diagnostic eolian features, these studies use a variety of petrological, geochemical and grain-size characteristics and compare them with well-known dust deposits from the Quaternary period, termed loess, to infer an eolian origin. However, in recent years, these methods have been challenged. Several studies have shown that deposits previously considered to be formed almost entirely by wind-blown dust derived from deserts, are instead predominantly water-laid (alluvial) and derived from local mountain ranges (Alonso-Zarza et al., 2009; Cheng et al., 2018; Liu et al., 2019). Here, we aim to solve these controversies by first reviewing the depositional environments of dust and critically assessing the traditional methods used to identify an eolian origin. Then, we present a clear set of methods which, when combined, will improve the recognition of dust in the geological record. Finally, we use the insights of our review to reinterpret the pre-Quaternary records of the Chinese Loess Plateau, which are considered as the longest and most continuous dust records in the world spanning the Neogene and arguably the Paleogene periods (e.g. An et al., 2014). Our review is limited to mineral dust in terrestrial records and excludes the marine realm. For a more detailed review on identifying dust from the Quaternary period, we refer to Muhs (2013), which includes lakes, marine records and ice cores.

2. Depositional environments of dust

In the following, we review the characteristics of loess, loessites and dust deposits in general.

2.1. Dust production, transport and deposition

The silt particles that constitute dust are generated by a wide variety of mechanisms including: abrasion of larger particles (by wind, in streams or by glaciers), chemical weathering, frost weathering in cold environments, salt weathering and aggregation of clay minerals in arid settings, biological production (e.g. diatoms, radiolaria, phytoliths and pollen) or inheritance from fine-grained parent rocks such as older mudrocks or metamorphic schists and phyllites (Potter et al., 2005; Pye, 1987; Muhs and Bettis, 2003; Wright, 2007). Glacial grinding has been proposed as an efficient silt producer during glacial periods (Smalley, 1966a; Smalley and Vita-Finzi, 1968), whereas desert processes such as salt weathering and abrasion by ephemeral streams or wind may dominate in arid environments (Crouvi et al., 2010; Pye, 1987; Tsoar and Pye, 1987; Whalley et al., 1982; Wright, 2001b). However, the efficiency of these desert processes is debated due to the lack of extensive dust deposits near vast deserts such as the Sahara and the Australian interior (Fig. 1; Smalley and Krinsley, 1978; Smalley, 1995). In addition, orogenies may play a major role in generating silt by: 1) fracturing minerals during exhumation, 2) the steep gradients resulting in high energy transport and abrasion, and 3) the high altitude climate promoting frost and salt weathering (Assallay et al., 1998; Pye, 1995; Smalley and Krinsley, 1978; Smalley, 1995; Sun, 2002; Wright, 2001a). The relative importance of these processes in producing large quantities of silt over various timescales remains unclear (Potter et al., 2005).

After production, the dust particles are entrained in the lower atmosphere by turbulent surface winds during storms and may remain

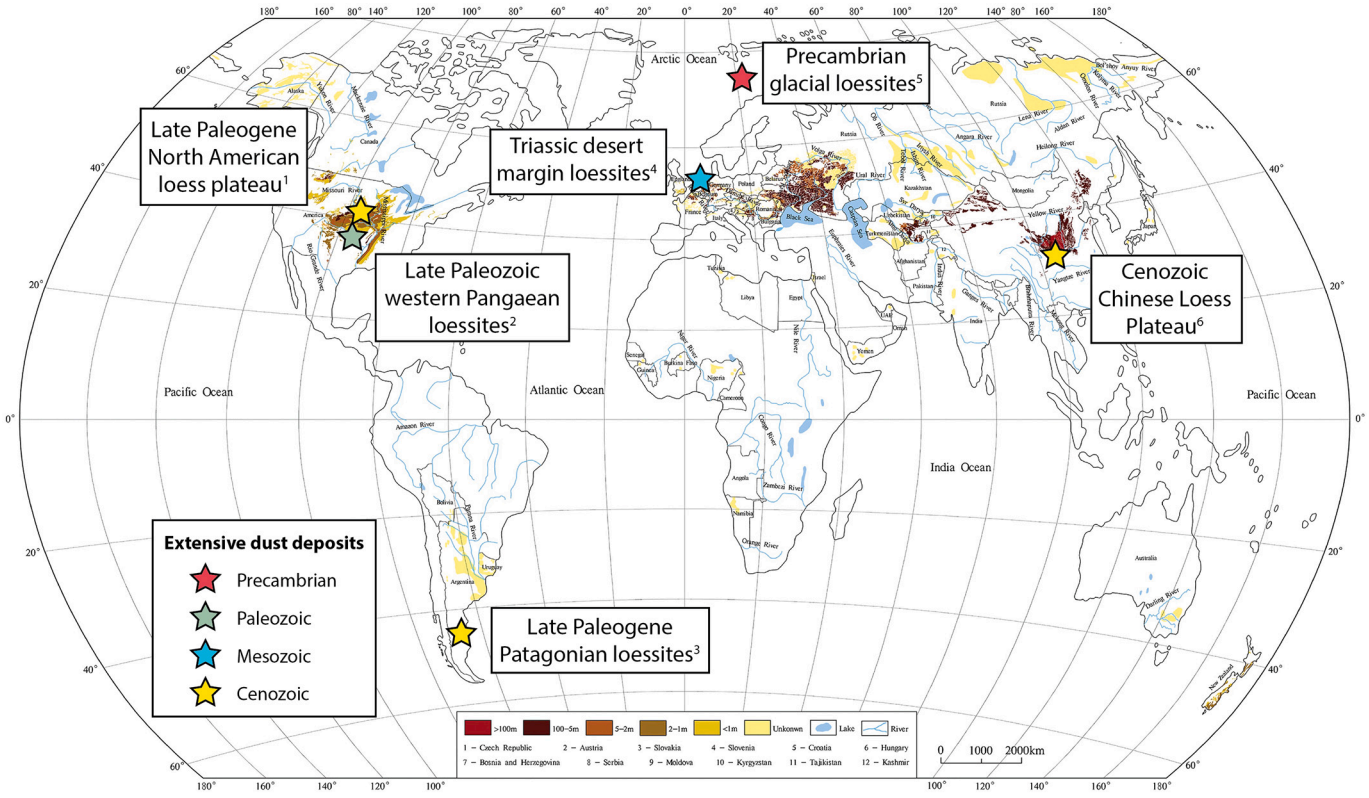

Fig. 1. Map of the global distribution of Quaternary loess deposits and thicknesses (modified from Li et al., 2020 and references therein). Stars indicate examples of extensive dust deposits from the pre-Quaternary: 1) Fan et al. (2020); 2) Johnson (1989); Soreghan et al. (2008); 3) Bellosi (2010); Selkin et al. (2015); 4) Jefferson et al. (2002); Wilkins et al. (2018); Wilson et al. (2020); 5) Edwards (1979); 6) An et al. (2014); Guo et al. (2002, 2008).

suspended until the wind speed and turbulence decrease and the dust settles (Fig. 2; Pye, 1987; Roe, 2009; Újvári et al., 2016). In general, grains finer than ~20 μm can remain suspended for longer and may travel thousands of kilometers when lifted up to the jet stream in the upper atmosphere (Fig. 2; Pye and Zhou, 1989; Sun, 2002; Sun et al., 2004; Vandenberghe et al., 2006). In addition, 'giant' mineral dust particles of >75 μm in diameter have been found to be transported over long distances as well, though the physical mechanisms underlying this transport remain unclear (van der Does et al., 2018). Dust transport via long-term suspension plays an important role in fertilizing the oceans with iron and thereby affecting the carbon cycle (Jickells et al., 2005; Martin, 1990).

Atmospherically transported dust particles may settle in a wide variety of both marine and terrestrial depositional environments, but need to be trapped to prevent subsequent deflation and to accumulate in the geological record. Efficient trapping mechanisms include surface obstacles such as vegetation and topography as well as wet surfaces such as lakes, oceans, ice caps, swamps and salt pans (Pye, 1995). After deposition, the dust particles may be reworked by water or significantly altered by pedogenesis, which obscures their eolian origin (e.g. Smalley, 1972; Smalley et al., 2009; Vandenberghe, 2013; Vandenberghe et al., 2018). Furthermore, the silt particles may have experienced a complex sedimentological history involving multiple steps of transport, deposition and reworking before being transported by dust storms (Li et al., 2020; Licht et al., 2016a; Muhs and Bettis, 2003; Pye, 1995; Smalley, 1966a; Wright, 2001a; Zheng, 2016).

This is exemplified by the dust deposits of the Chinese Loess Plateau where provenance studies have revealed a complex network of transport pathways ultimately resulting in the deposition of dust on the Plateau (Fig. 3). This dust was traditionally thought to originate from the interior deserts, but recent provenance studies show that the silt is mainly derived from the northern Tibetan Plateau with some additional contributions from the Central Asian orogeny (including the Tian Shan and the Gobi-Altay; see review in Sun et al., 2020). In this view, the deserts draining these mountain ranges are acting as a transient storage for the alluvial mountain silt to be reworked as loess, rather than a significant source of silt (Assallay et al., 1998; Li et al., 2020; Smalley, 1995; Sun, 2002). Accordingly, Derbyshire et al. (1998) noted that the alluvial fans north of the Tibetan Plateau provide an important source of silt for modern-day dust storms in central China. The Yellow River is also shown to be of major importance in transporting material from the Tibetan Plateau to floodplains in the north, where the silt can subsequently be reworked by dust storms (Fig. 3; Bird et al., 2015; Stevens et al., 2013; Licht et al., 2016a; Nie et al., 2015). Some of these studies recognized an additional input of deflated material from the Qaidam Basin during colder glacial periods due to a stronger influence of the low-level westerlies (Fig. 3; Kapp et al., 2011; Licht et al., 2016a; Pullen et al., 2011). These studies demonstrate that the deposition of dust may only be the latest step in a complex history of sediment transport, which has important implications for the petrological and geochemical characteristics of the dust particles.

2.2. Loess and loessites

Dust particles bigger than ~20 μm start to settle as the turbulence in the lower atmosphere decreases, forming blankets of dust which are fining and thinning away from the source due to selective transport (Fig. 2; Pye, 1987; Pye and Zhou, 1989). These bodies composed entirely of terrestrial dust are termed loess (Pye, 1995) and are well known from the Quaternary period covering substantial portions of the Earth's surface (Fig. 1; Li et al., 2020). Loess can be recognized as buff coloured deposits of loosely-packed silt-sized grains forming steep vertical outcrops (Fig. 4 A). The sedimentary structure is massive, but may contain burrows and fractures. Primary structures such as vague horizontal or cross-laminations are observed only in rare cases (e.g. Muhs, 2013). Other characteristic features of the Quaternary loess are the interbedded fossil soils (paleosols), which can be readily identified in the field as laterally extensive, reddish-brown layers (Fig. 4 B). These paleosols are enriched in fine-grained phyllosilicates occurring as clay coatings due to chemical weathering (e.g. Maher, 2016; Muhs and Bettis, 2003).

The lack of primary sedimentary structures in loess resulted in controversies dating back to the nineteenth century regarding the origin of these deposits (Pye, 1987; Smalley et al., 2001; Richthofen, 1882). Massive silt beds are common in various depositional environments including alluvial, lacustrine, eolian and marine settings. Additionally, it has been proposed that loess may have formed by in-situ weathering of the underlying material (e.g. Pécsi, 1990). Richthofen was one of the early proponents arguing for an eolian origin and listed numerous observations from the Chinese Loess Plateau to support his case (Smalley et al., 2001; Richthofen, 1882). These include the common occurrence of rootlets, land snails and mammal fossils indicating a terrestrial environment. Furthermore, the distinctly different composition of loess compared to the underlying bedrock suggests transport from elsewhere, rather than in-situ weathering. The most convincing evidence for an eolian nature of this transport is the sheet-like draping of loess bodies covering the underlying topography and resulting in undulating surfaces found over a wide altitudinal range (Muhs, 2013; Pye, 1987; Richthofen, 1882). Pye (1987) adds that the loose packing and associated high porosity of loess is an additional characteristic for eolian silt. Furthermore, the geographic relationship between the pathways of modern-day storm tracks and the fining and thinning of loess bodies further corroborates their eolian origin (Pye, 1987). However, these observations are of limited use when studying older geologic records, because burial diagenesis affects porosity, the paleotopography is rarely preserved and ancient atmospheric pathways are unknown.

Nevertheless, lithified pre-Quaternary deposits sharing the

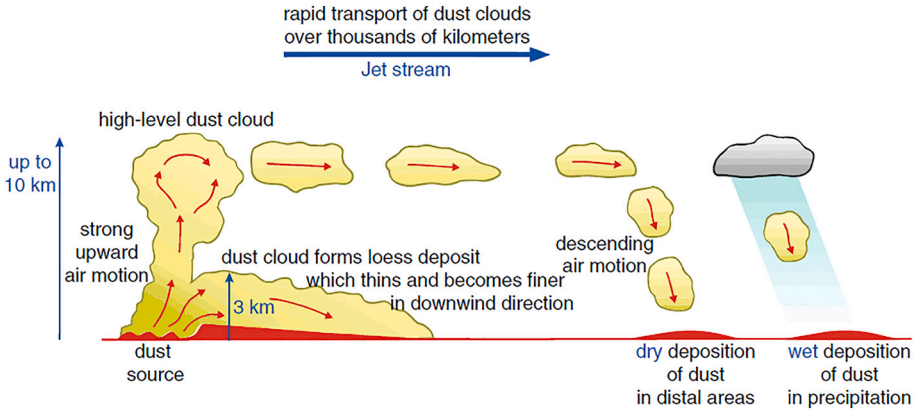

Fig. 2. Schematic diagram showing atmospheric low- and high-level dust transport. Figure redrawn from Pye and Zhou (1989) by Knippertz and Stuut (2014).

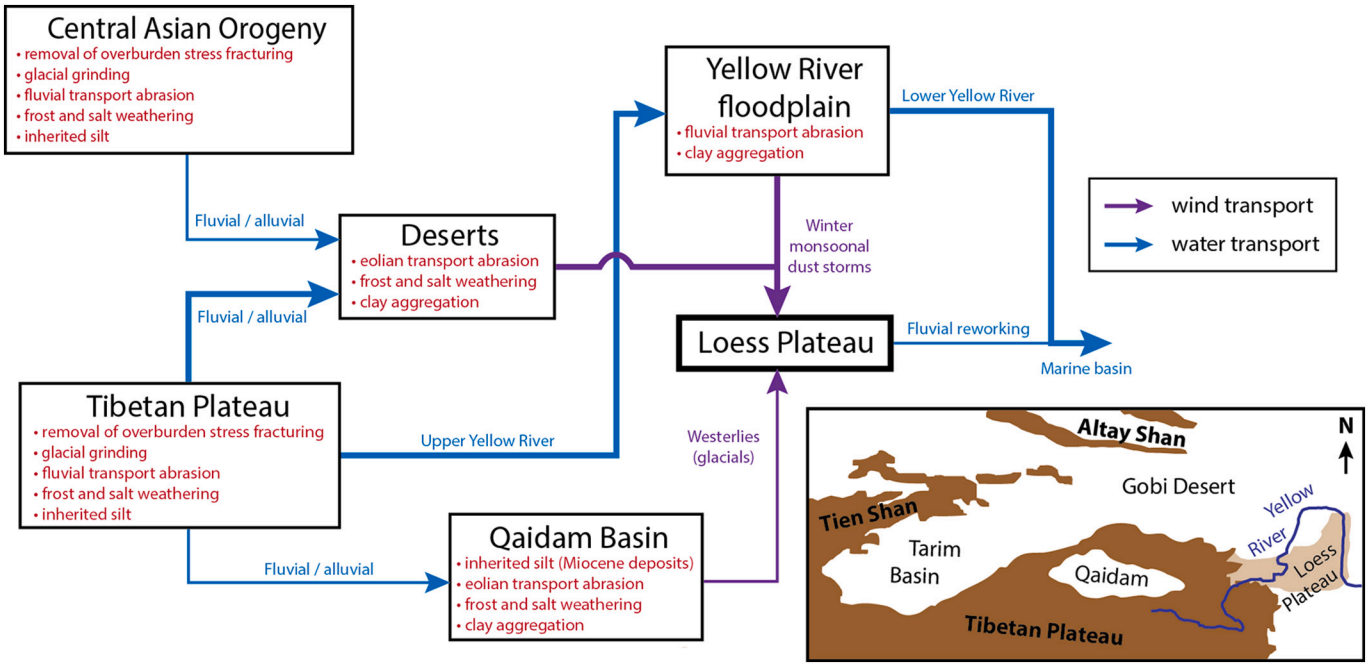

Fig. 3. Schematic overview of predominant transport pathways that result in the deposition and reworking of the Chinese Loess Plateau. Silt producing mechanisms are indicated in red, transport by water in blue and transport by wind in purple. Note that the transport of fine-grained dust by the upper-level westerly jet stream is not included in this diagram. Inset map shows the main geographic features of the northeastern Tibetan Plateau region. (For interpretation of the references to colour in this figure legend, the reader is referred to the web version of this article.)

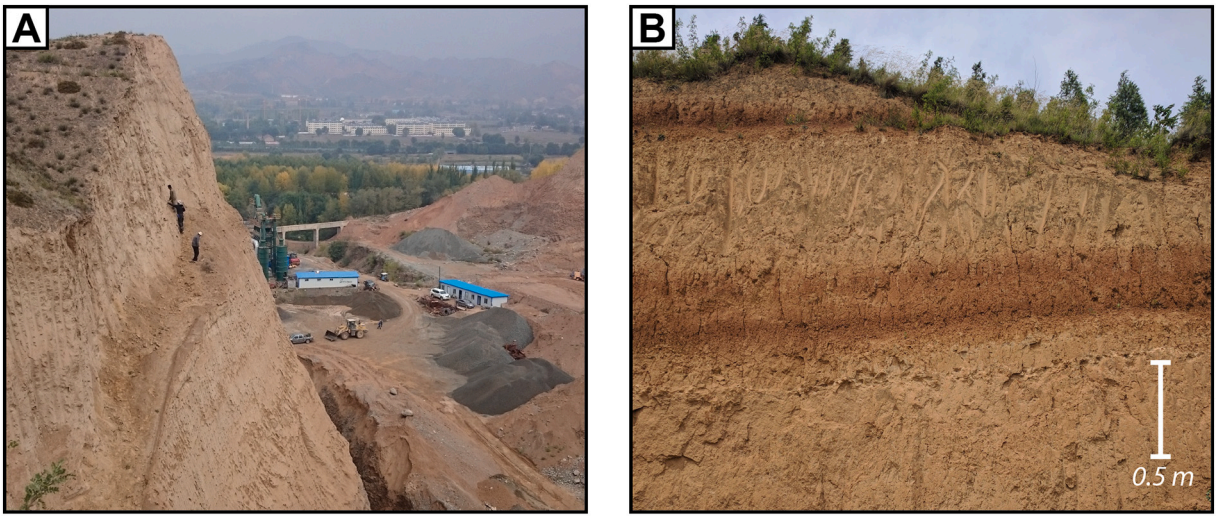

Fig. 4. Pictures of Quaternary loess from: A) Ledu (Xining Basin) in the westernmost Chinese Loess Plateau, person at outcrop for scale. B) Xi'an in the south-central Chinese Loess Plateau.

characteristics of modern loess have been observed and interpreted as dust-blown deposits. These strata are termed loessites (Pye, 1995) and have been identified using the following criteria: 1) massive sedimentary structure showing no evidence of alluvial or lacustrine deposition (e.g. Ding et al., 1998a; Guo et al., 2002; Johnson, 1989; Wilkins et al., 2018), 2) homogeneous silt-sized grain-size distributions due to selective transport (e.g. Carrapa et al., 2015; Fan et al., 2020; Guo et al., 2001, 2002; Li et al., 2018; Licht et al., 2014; Lu et al., 2001; Sun et al., 2010; Wasiljeff et al., 2020; Yang and Ding, 2004; Zheng et al., 2015), 3) angular shapes of the quartz grains, as well as other surface morphology features indicating eolian transport (e.g. Carrapa et al., 2015; Edwards, 1979; Fan et al., 2020; Guo et al., 2001, 2002; Li et al., 2018; Liu et al., 2006; Licht et al., 2014; Wang et al., 2016a), 4) provenance signals similar to the Quaternary loess including major, minor and rare earth elemental compositions, as well as Nd isotopes and detrital zircon U-Pb (e.g. Garzione et al., 2005; Guo et al., 2002; Li et al., 2018; Licht et al., 2016b; Jiang and Ding, 2010; Sun et al., 2010; Sun and Windley, 2015; Wang et al., 2014; Wang et al., 2016a), 5) magnetic fabric similar to Quaternary loess (Liu et al., 1988), 6) geographic relations between the supposed source of the dust and the dust bodies as observed in grain-size and thickness of the deposits (Miao et al., 2004; Yang and Ding, 2004), 7) low accumulation rates (Ding et al., 1998b; Garzione et al., 2005; Sun et al., 1998a) and 8) the occurrence of land snail fossils (Li et al., 2006a).

Another commonly used argument in identifying loessites is the absence of alternative depositional models to explain the occurrence of massive silt-sized deposits in the terrestrial realm (e.g. Johnson, 1989).

However, several studies have proposed a distal mudflat/floodplain involving predominantly alluvial deposition as an alternative to exclusively windblown deposits (Alonso-Zarza et al., 2009, 2010; Flynn et al., 2011; Li et al., 2006b; Liu et al., 2019; Zhang et al., 2013). In the following, we will present this mudflat depositional model.

2.3. Mudflat depositional model

Deposition on terrestrial mudflats involves predominantly alluvial transport in a low-relief basin, which would enable extensive suspension settling of fine-grained material in a fluvio-lacustrine environment (Fig. 5; Donselaar et al., 2013; Smoot and Lowenstein, 1991; Talbot et al., 1994; van Toorenenburg et al., 2018). This is especially common in arid to semi-arid settings and endorheic basins where downstream evapotranspiration and percolation may result in the subaerial termination of rivers on the floodplain rather than in lacustrine delta's (Donselaar et al., 2013). Modern analogues for these sedimentary systems include the Altiplano Basin in Bolivia (Donselaar et al., 2013; van Toorenenburg et al., 2018) and the continental interior of Australia (Talbot et al., 1994).

Most of the sediments in this setting are derived from the local mountain ranges forming proximal alluvial fans and scree deposits containing breccias, conglomerates and sandstones. Fluvial channels, either ephemeral or perennial, transport the sediment to the more distal regions of the basin where the finer material is deposited on extensive mudflats via terminal fans, crevasse splays and overbank suspension settling during episodic floods. These flooding events are able to inundate vast areas due to the low gradient of the basin and lakes or salt pans may be found at the distal ends of this sedimentary system. The transition from proximal to distal sediments may occur rapidly. For example, the proximal sands in the Australian interior are observed to extend only one kilometer from the valley mouth into the basin and subsequently grade to open plains consisting predominantly of mud (Talbot et al., 1994). An additional input of windblown dust to the mudflat may occur as well, either from an extrabasinal source or by deflation and redeposition of local sediments. The latter is especially prevalent because most mudflats occur in arid to semi-arid environments and provide ample loose silt for eolian reworking. Fine-grained material entering mudflat systems can alternate multiple times between fluvial transport and eolian transport (Hardie et al., 1978), which makes the identification of "true" dust deposits difficult.

This mudflat model involves alluvial, fluvial, lacustrine and eolian deposits and thereby provides an explanation for the co-occurrence of lacustrine siltstones, fluvial sandstones, and loess-like siltstones in numerous locations (e.g. Alonso-Zarza et al., 2009, 2010; Flynn et al., 2011; Guo et al., 2010; Liu et al., 2019). Yet massive terrestrial siltstones are commonly interpreted as loessites which implies deposition almost exclusively by wind. In the following, we will show that the loess-like features listed in Section 2.2 may also occur via other modes of deposition on a terrestrial mudflat and therefore cannot be unambiguously linked to dust deposition alone.

2.4. Alluvial origin for massive terrestrial siltstones

The massive sedimentary structure observed in siltstones is often cited as characteristic for eolian deposition and is indeed similar to the Quaternary loess. However, it can be formed by different mechanisms as well. Modern observations show that clay and silt may aggregate to form sand-sized particles that are transported as bedload in fluvial systems or by wind to form lunettes (Rust and Nanson, 1989; Smoot and Lowenstein, 1991; Talbot et al., 1994; Wright and Marriott, 2007). Subsequent burial disaggregates these particles resulting in a massive sedimentary structure. In addition, post-depositional processes such as bioturbation, mud-cracking or pedogenesis may occur on subaerially exposed mudflats and rework the original sedimentary structures resulting in massive mud- and siltstones with only vaguely recognizable laminations (Talbot et al., 1994; Smoot and Olsen, 1988).

Another indicator for dust is the uniform loess-like grain-size distribution. However, even the Quaternary loess shows a wide variety of poorly-sorted grain-sizes depending on the source, distance to the source and pedogenic overprint (Fig. 6 A; Pye, 1995; Újvári et al., 2016; Vandenberghe, 2013; Vandenberghe et al., 2018). A commonly accepted example of pre-Quaternary loess deposits are the Red Clay strata of central China (e.g. An et al., 2001, 2014). However, the grain-size distributions of the Red Clay are finer than Quaternary loess (Fig. 6 B, C) and more similar to those found on the alluvial mudflat of the Altiplano Basin (Fig. 6 D; van Toorenenburg et al., 2018). This shows that the grain-size distributions alone are not a good indicator for eolian transport. Lu et al. (2001) used the empirical Y-value, which is based on various grain-size characteristics including the mean, sorting, kurtosis

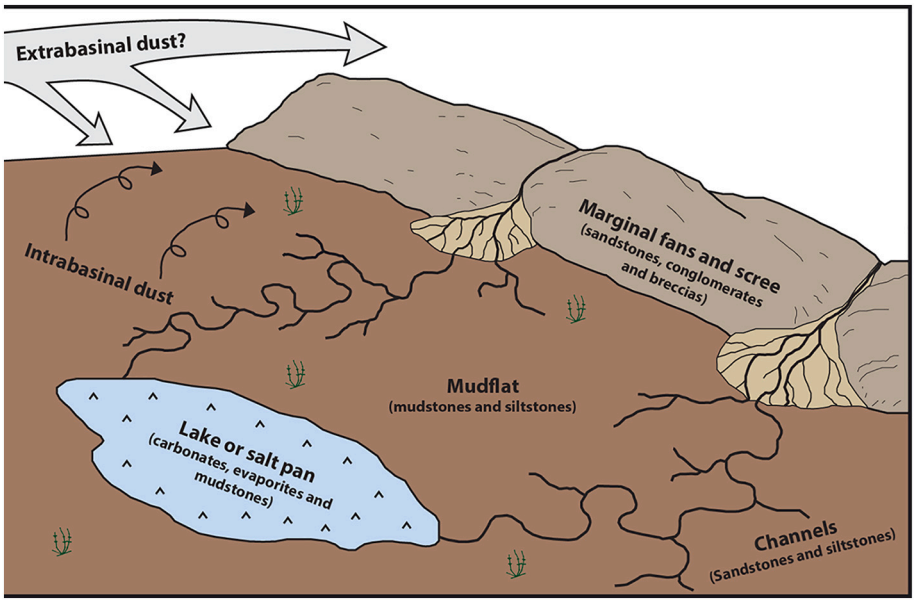

Fig. 5. Alternative depositional model for loessites involving a low-relief basin resulting in alluvial deposition on an extensive mudflat. In addition, eolian deposition may occur by reworking local sediments or atmospheric transport of extrabasinal dust. Redrawn from Talbot et al. (1994).

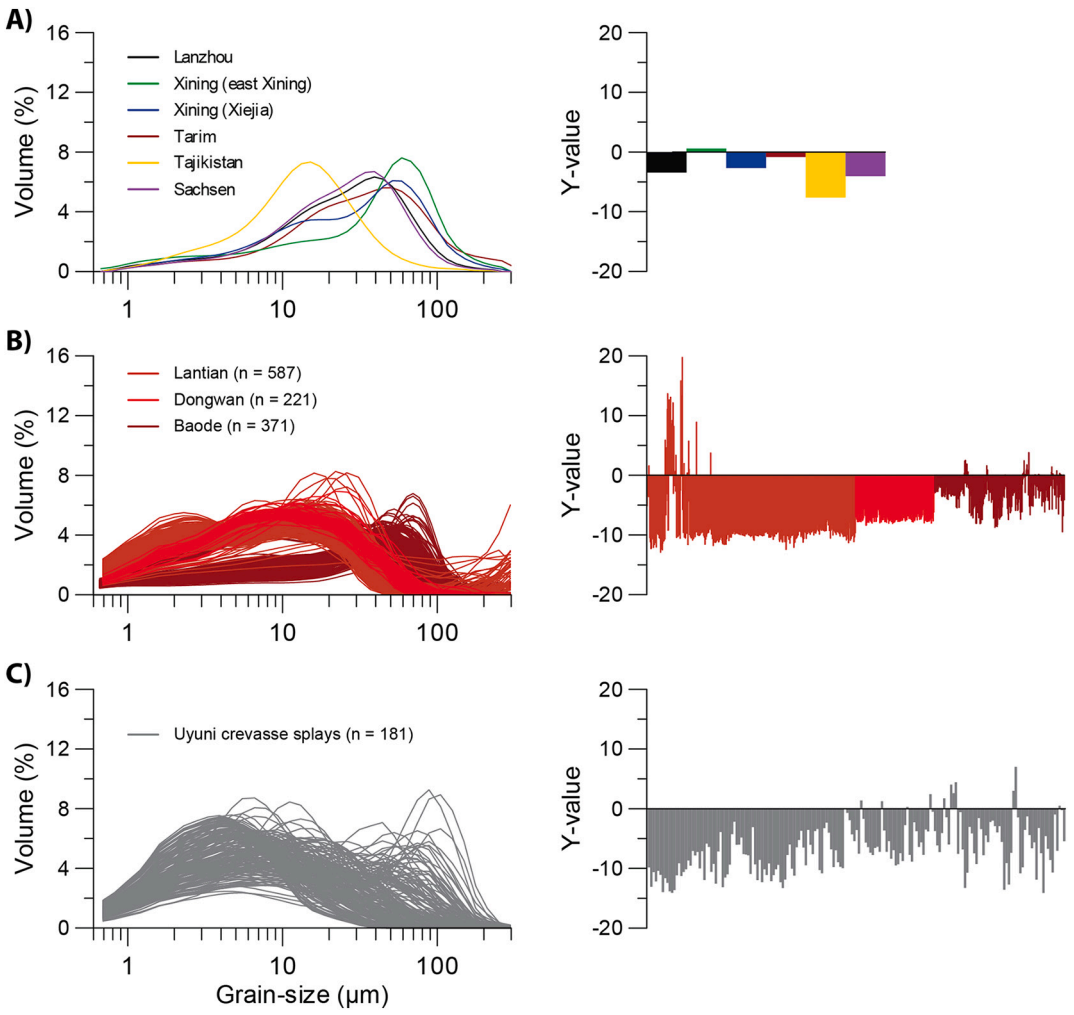

Fig. 6. Grain-size distributions and Y-values calculated using the mean, sorting, skewness and kurtosis derived using the logarithmic moment method as implemented in Gradistat (Blott and Pye, 2001) and the Y-value equation of Lu et al. (2001) of: A) Quaternary loess from a variety of locations (measured using the same methods as in Meijer et al., in review); B) Mio-Pliocene Red Clay from the southern (Lantian), western (Dongwan) and northeastern (Baode) Chinese Loess Plateau (Shang et al., 2016); C) Crevasse splay deposits from the modern-day Altiplano Basin mudflat (van Toorenenburg et al., 2018). Note that the grain-size distributions shown here are derived from various studies using different pre-treatments, laser diffractors and optical parameters that may also incur slight variations (Varga et al., 2019a). (For interpretation of the references to colour in this figure legend, the reader is referred to the web version of this article.)

and skewness, to distinguish eolian deposits with a negative Y-value from alluvial deposits which have a positive Y-value. However, most of the alluvial mudflat grain-size distributions shown here have negative Y-values as well, which indicates that this is not a reliable tool for identifying eolian deposits (Fig. 6).

The angular shape of the silt-sized quartz grains is proposed to be evidence of loess and is linked to eolian transport. Newly weathered quartz grains derived from granites tend to form sand-sized particles due to crystallographic constraints (Smalley, 1966b). To create silt-sized quartz, these grains need to be broken and the resulting angular shape is therefore due to abrasional processes rather than an indication of eolian transport (Pye, 1987). Furthermore, the conchoidal fractures observed on the surface of the quartz grains (e.g. Liu et al., 2006) may be found in a variety of depositional environments and alone are not diagnostic of eolian transport (Vos et al., 2014).

Geochemical provenance signatures showing similarities with the overlying Quaternary loess have been used as evidence for windblown transport, but also to derive paleowind directions, especially when linked to extrabasinal sources. However, as shown in Section 2.2, dust deposits may experience a complex sedimentological history including both alluvial and eolian reworking (Fig. 3). The geochemical properties can thus be expected to be similar for both the eolian and alluvial sediments and are not necessarily diagnostic for either one. Furthermore, the REE patterns which are often cited as evidence for eolian transport are merely an indication of a multi-recycled and well-mixed sediment (Gallet et al., 1998) rather than eolian dust. Interestingly, Wang et al. (2014) show a loess-like geochemistry for the siltstones interbedding the fluvial sandstones that underlie the Chinese Loess Plateau. They use this as evidence to propose that these silts should be regarded as dust as well, but alternatively it could indicate that both alluvial and eolian siltstones have a similar geochemistry, especially because both are ultimately derived from the Tibetan Plateau (Fig. 3). Furthermore, it should be noted that most bulk geochemistry studies only compare with the Quaternary loess and imply long-range extrabasinal dust transport while failing to assess the influence of intrabasinal sources. More recent provenance studies using U-Pb signatures from detrital zircons and heavy mineral assemblages show significant contributions from local mountain ranges. The zircon age distributions of the Dongwan and Chaona Red Clay sections show strong similarities with the neighboring Liupan Shan (Nie et al., 2014; Shang et al., 2016), whereas the Lantian and various sections in Tianshui Basin indicate the neighboring Qinling Shan as the predominant source (Liu et al., 2019; Zhang et al., 2018;). This may indicate that local alluvial transport plays a major role rather than large-scale extrabasinal dust fluxes (Liu et al.,

2019).

Liu et al. (1988) used the magnetic fabric to distinguish eolian from alluvial strata. But this method is of limited use because the magnetic mineral assemblage and tectonic strain varies through time which alters the magnetic fabric (Borradaile and Henry, 1997). Other studies have used basin-scale correlations between records to identify trends in grain-size and thickness. However, whether these can be linked to proposed dust sources or alluvial material derived from local mountain ranges remains debated (Ding et al., 2000; Liu et al., 2019; Miao et al., 2004; Yang and Ding, 2004). Furthermore, both the low accumulation rates and the occurrence of terrestrial snails are not diagnostic of eolian transport and can be observed on alluvial mudflats as well.

In conclusion, the evidence used to identify loess in pre-Quaternary records cannot exclude alternative interpretations involving alluvial deposition of silt on extensive low-gradient mudflats. This is supported by the co-occurrence of fluvial sandstones and lacustrine mudstones which would suggest various modes of deposition, in contrast to the exclusively windblown bodies of loess observed in the Quaternary period. Dust deposition may occur on these mudflats as well, but should be regarded among other alluvial sediment contributions (Fig. 5).

3. Methods to identify dust in the geological record

We synthesize here a set of existing methods which, when combined, enable a reliable identification of dust in the geological record while acknowledging additional alluvial components. First, quartz surface morphology analysis enables the identification of the transport modes for the various grains and distinguishes eolian from alluvial components. Second, detailed provenance analysis enables to distinguish local reworked sediments from extrabasinal components which, in the case of dust, may aid in reconstructing atmospheric pathways and dust fluxes. Third, end-member analysis of grain-size and -shape distributions enables to quantify the various sedimentary contributions in the records. And finally, additional paleoenvironmental and basin analyses may be used to strengthen the interpretations regarding an eolian origin.

3.1. Quartz surface morphology

Particle collisions during transport result in characteristic nm- to µm-scale features on the grain surfaces. These features are largely dependent on the fluid viscosity of the transporting medium and can therefore be used to distinguish sediment transport in wind and water. The analysis of these surface morphologies has been applied to quartz grains in particular, because of their high abundance (e.g. Krinsley and Takahashi, 1962; Vos et al., 2014). Consequently, quartz surface morphologies have been extensively described using a scanning electron microscope (SEM) on grains from a variety of both modern and ancient sedimentary environments, as well as on artificially-produced quartz grains subjected to various transport conditions in the lab (e.g. Costa et al., 2013; Keiser et al., 2015; Krinsley and Takahashi, 1962; Nieter and Krinsley, 1976; Vos et al., 2014). For a more detailed review on the sample preparation, SEM handling and surface morphology descriptions we refer to Vos et al. (2014) and references therein.

In general, the impacts by wind are of higher energy than subaqueous collisions which are cushioned by the surrounding water. The latter are therefore characterized by µm-scale, v-shaped percussion marks, whereas eolian impacts result in larger conchoidal fractures separated by meandering ridges, crescentic percussion marks and dish-shaped depression (Fig. 7). Furthermore, higher energy eolian collisions result in the shattering of the quartz crystal lattice and create a highly reactive surface of amorphous silica with adhering nm-scale particles and thin parallel upturned plates, both composed of silica (Fig. 7; e.g. Krinsley and Trusty, 1985; Vos et al., 2014). Identification of these features therefore enables us to distinguish between an alluvial and an eolian mode of transport and can be applied to identify dust in the geological record (e.g. Licht et al., 2014; Fan et al., 2020). Careful quantification of these surface morphological features may even indicate the relative importance of various transport mechanisms for grains that have

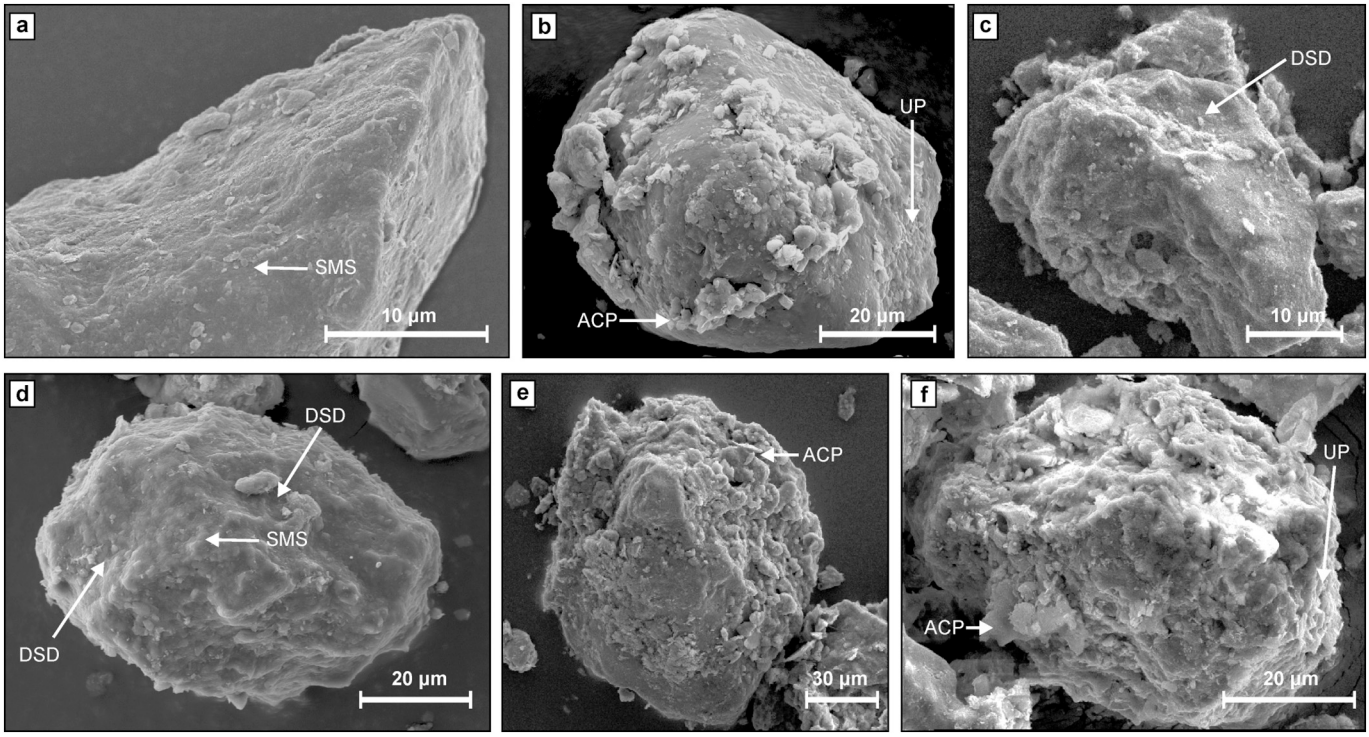

Fig. 7. SEM images of quartz grains from the late Eocene strata of the Xining Basin showing morphological features resulting from high impact collisions and indicating eolian transport. These features include dish-shaped depressions (DSD), smooth surfaces (SMS), adhering clay-sized particles (ACP). Figure is reproduced from Licht et al. (2014).

experienced multiple modes of transport. In addition, the identification of overprinting relations between these morphological features may help to derive the sequential order of the various transport modes (Vos et al., 2014), which is especially useful for loess-like materials characterized by both alluvial and eolian deposition and reworking (Fig. 5).

However, it should be noted that most of the eolian surface morphologies described above have been identified on sand-sized quartz grains which are transported by saltation and creep, whereas silt-sized dust of <50 μm is transported in suspension (e.g. Újvári et al., 2016). Furthermore, silt-sized grains may not have enough momentum for the high energy impacts needed to create the typical eolian surface morphologies. So far, only few studies have focused on the surface morphologies of silt-sized quartz grains. Krinsley and McCoy (1977) note that most silt-sized quartz grains are fragments of broken sand-sized grains. They suggest that even though the silt-sized material may not create characteristic surface morphologies, the silt may still record useful surface textures on the surfaces of the original sand-sized grain preserved on some of the silt particles after fragmentation. Other studies have noted significant differences between the quartz morphologies of loess and eolian sand. The shape of the latter is rounded and characterized by bulbous edges (e.g. Krinsley and Trusty, 1985; Vos et al., 2014), whereas silt-sized quartz from loess deposits is subangular to subrounded with sharp edges and flat cleavage surfaces (Krinsley and Smalley, 1973; Nieter and Krinsley, 1976; Pye, 1987). Other more delicate features such as polygonal cracks formed by salt weathering are more common on silt-sized particles and rarely observed on sand-sized grains because the cracks are easily abraded by the higher energy impacts of saltation compared to transport in suspension (Pye, 1987; Vos et al., 2014). Adhering nm-scale particles are observed in loess as well (Pye, 1987) and may be a diagnostic feature, because wind tunnel experiments show that eolian-transported silt creates adhering silica particles due to abrasion (Nieter and Krinsley, 1976). However, Pye (1987) notes that the composition of the adhering particles in loess consist of illite, kaolinite and calcite of pedogenic origin as well as silica and therefore careful compositional analysis is required before interpreting the adhering particles as eolian features.

Quartz surface morphology analysis provides a strong tool to derive transport modes and identify dust in the geological record. Diagenetic overprinting may hamper the analysis for deposits older than the Mesozoic, but can be easily recognized as crystal overgrowths (Vos et al., 2014). Furthermore, the method may be biased by the expertise of the user in recognizing characteristic surface features but recent image analysis tools may aid in automating this process (Říha et al., 2019). However, extensive data is required for training these algorithms, but has been lacking for the silt-sized domain. Future work should therefore focus on describing quartz silt from a variety of sedimentary transport processes to bring the current surface morphology knowledge up to date with the sand-sized grains.

3.2. Provenance

Provenance studies play an important role in deriving the source regions of the dust and in assessing the intra- and extrabasinal contributions. In addition, these studies are widely used to derive atmospheric transport pathways (e.g. Soreghan et al., 2002, 2014). However, it should be emphasized that the provenance signal itself is no evidence for eolian deposition and should be used together with other data. Only when a clear extrabasinal source is identified in the absence of a fluvial connection to the deposits, can the provenance signal be used as proof for eolian transport. Still, it would remain unclear whether this mode of transport was the last step of sediment transport because the material could have been subsequently reworked. On the other hand, a local provenance is not exclusive to alluvial deposits and may result from wind erosion of nearby outcrops (e.g. Kapp et al., 2015).

Sun et al. (2020) provide an extensive review of provenance tools which have been used on the Chinese Loess Plateau but are also applicable to other dust records and will be summarized in the following. These tools can be subdivided in tracers derived from a single type of mineral or from an assemblage of various minerals. Single-mineral tracers include the various characteristics of quartz minerals such as $\delta^{18}O$, Electron Spin Resonance (ESR) and Crystallinity Index (CI), which are controlled by the age and temperature at the formation of the minerals. Another widely used single-mineral tracer is the U-Pb age spectra of detrital zircon grains. Mineral-assemblage tracers include elemental ratios, isotopic signatures of Sr-Nd-Pb-U, Hf-Th and Re-Os, magnetic properties and heavy mineral composition. Preferably, multiple tracers should be used to identify the provenance more accurately.

Elemental ratios and isotopic signatures are generally measured on bulk samples, which has the advantage of considering the entire range of minerals and grain-sizes in the material (Bird et al., 2020). On the other hand, these bulk signatures perform poorly in sediments with mixed sources because the provenance signatures average out. To overcome this limitation, the signatures should be characterized for grain-size fractions or individual grains representing the various sources and modes of sediment transport. One of these methods applied to individual grains is measuring the U-Pb age spectra of zircons, which accurately distinguishes mixtures of various sources if a large enough number of grains are measured (Licht et al., 2016a). In addition, robust minerals such as zircons and quartz are less affected by post-depositional weathering and are therefore preferred over other minerals or bulk analyses. In the future, the use of other minerals such as titanite and rutile may be explored for U-Pb age spectra as well.

Provenance methods measuring the isotopic ratios of individual grains are limited to relatively large grains of often >40 μm due to the amount of material required via laser ablation. Neglecting the smaller grain-sizes introduces a size bias (e.g. Bird et al., 2015), but future technical developments may improve these limitations. This would enable characterizing the elemental and isotopic signatures of individual grains, rather than bulk measurements and would significantly improve the recognition of various source regions in mixed sediments.

3.3. End-member analysis of grain-size distributions

Uniform grain-size distributions in the silt domain are used to identify dust in geological records. However, these are of limited use due to the wide variety of overlapping grain-sizes occurring in both dust and other alluvial environments (Fig. 6). Furthermore, these distributions are rarely unimodal, but rather contain a multimodal mix representing grain-size fractions derived from various sources and sorted by distinct transport mechanisms. Unmixing these grain-size distributions enables the quantification of these various components within the sedimentary record (Fig. 8). This is especially useful for studying sedimentary

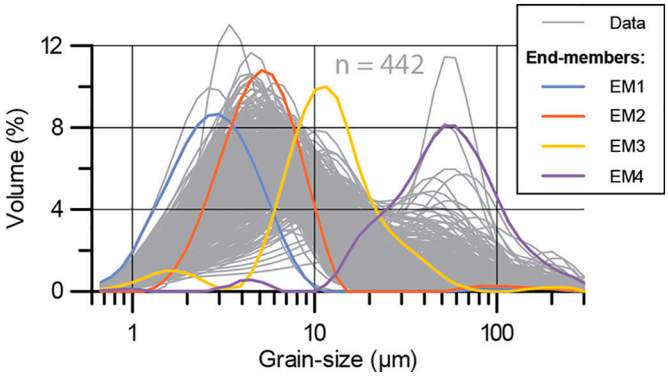

Fig. 8. End-member analysis of grain-size distributions from Eocene mudflat deposits in the Xining Basin. Data and methods are reported in Meijer et al. (in review). EM4 is interpreted as dust based on quartz surface morphologies (Licht et al., 2014) and provenance (Licht et al., 2016b).

environments with multiple depositional modes such as on a low-relief mudflat (Fig. 5).

Various methods can be used to unmix grain-size data including parametric curve-fitting and end-member modelling (Varga et al., 2019b). Parametric curve-fitting uses predefined functions of distributions and fits these with the measured grain-size distributions in the geological record to quantify their relative abundance (Paterson and Heslop, 2015; Sun et al., 2002; Wu et al., 2020). The accuracy of this analysis depends on the predefinition of the fitting functions and is especially useful for modern and recent geological records, in which the potential sources are well constrained. However, on longer geological timescales, knowledge of the grain-sizes in the various sources is usually limited. Therefore, non-parametric end-member modelling is a more appropriate method (Weltje and Prins, 2007). End-member modelling uses an algorithm that considers the entire grain-size dataset of the record to construct multiple end-member distributions in which the dataset can be optimally decomposed (Fig. 8). In recent years, various end-member algorithms have been developed and shown to perform well using artificial and natural datasets (Dietze and Dietze, 2019; Paterson and Heslop, 2015; van Hateren et al., 2018; Varga et al., 2019b).

End-member modelling has been successfully applied to distinguish eolian and alluvial contributions in marine cores (Weltje and Prins, 2003) and lacustrine records (Dietze et al., 2014; Rits et al., 2016) as well as various dust components in Quaternary loess (Nottebaum et al., 2015; Prins et al., 2007) and Neogene Red Clay (Shang et al., 2016: Xu et al., 2018). However, it should be noted that the end-member grain-sizes themselves provide limited sedimentary information and should be combined with other data such as quartz surface morphology and provenance to interpret their sedimentary origin. After interpreting the origin of the end-members, their contributions can be quantified throughout the studied records.

Various techniques can be used to measure grain-size distributions, but laser diffraction is the most widely used for silt-sized sediments because of the high reproducibility and measurement speed (Goossens, 2008). This technique measures the grain-size distribution indirectly by converting the diffraction pattern of a laser beam passing through the suspended particles. The accuracy of the measurements depends on the optical parameters used for the conversion and may vary between different laser diffractors (Varga et al., 2019a). A more direct but time consuming measurement of the grain-size distributions can be obtained by using dynamic image analysis, which simultaneously provides additional data on the grain-shapes (Shang et al., 2018; van Hateren et al., 2019; Varga et al., 2018). These combined size and shape characteristics may aid to better define the end-members (van Hateren et al., 2019). Furthermore, a Raman spectroscope can be coupled to the optical microscope to determine the mineral properties of the studied particles (Szalai et al., 2019). Since sediment transport is controlled by the size, shape and density (and therefore mineralogy) of the particles, constraining these three parameters in one single analysis will benefit the characterization of both dust and other components in the sedimentary record.

3.4. Stratigraphic and basinal analysis

For significant dust deposition to occur, an effective source, sink and transport mechanism are needed (Pye, 1995). The source should provide ample of loose, silt-sized material available for transport and the sink should contain a trap, such as vegetation, a wetted surface or topographic obstacle to contain the dust. Additional sedimentological, stratigraphic and biological data may therefore be used to assess the capacities of both the source and sink (e.g. Vandenberghe et al., 2018). In settings where the sink has a different bedrock lithology than the dust source, it is especially convenient to recognize allogenic dust components (e.g. Muhs, 2013). Quaternary examples include the identification of quartz grains in the basaltic soils on Hawaii (Begét et al., 1993) and in a volcanic maar in Japan (Xiao et al., 1997). In settings involving chemically- or biologically-formed sediments it is similarly convenient to recognize and quantify siliciclastic dust components. For example, Permian dust accumulation rates have been derived from coal beds by measuring the titanium content assumed to be a proxy of dust (Large and Marshall, 2015; Marshall et al., 2016).

Furthermore, it should be noted that individual geological records reflect only the depositional environment of a specific location. This environment is partly constrained by the basin configuration and surrounding topography. Records located near the basin margin may contain abundant alluvial material derived from the neighboring mountain ranges, whereas windblown dust may accumulate in records located in a more distal setting. Individual records may be hindered by local autogenic variability related to splays, storms, events, and channels moving, eroding and/or redepositing sediments (e.g. Hajek and Straub, 2017). As such, a single record is limited for a robust evaluation of dust deposition and a basin-scale analysis is required instead. The use of multiple records to derive a regional or even global imprint of paleorecords is common practice in marine studies. Long-term stable carbon and oxygen isotopes series have been stacked to reduce the local noise and disturbances since considerable time (e.g. Hays et al., 1976; Lisiecki and Raymo, 2005). Similar methods have been applied to Quaternary loess records (e.g. Liu and Ding, 1998), but should be used for pre-Quaternary dust records as well.

4. The geological record of the Chinese Loess Plateau

Using the considerations discussed above, we reassess the geological record of the Chinese Loess Plateau located in north-central China where dust has accumulated for millions of years (Fig. 9). The Loess Plateau has therefore provided an invaluable record for studying paleoenvironmental changes in the terrestrial realm, especially during the Quaternary period (see reviews in: An et al., 2014; Liu and Ding, 1998; Maher, 2016; Porter, 2001). In recent years, this dust record has been expanded to include the underlying siltstones of increasingly older ages (Fig. 9). These strata cover the Pliocene-Miocene epochs in the eastern Loess Plateau (An et al., 2001; Ao et al., 2016; Qiang et al., 2001; Sun et al., 1998a, 1998b; Wang et al., 2014; Xu et al., 2009), the Miocene-Oligocene in the west (Guo et al., 2002; Qiang et al., 2011), and the Eocene in the westernmost part of the Loess Plateau (Licht et al., 2014). In the following, we will review the nature of these deposits and challenge the exclusively eolian origin of the pre-Quaternary strata.

4.1. Quaternary loess

The Chinese Loess Plateau covers a wide area of $\sim 4.4 \times 10^5$ km^2 with Quaternary dust ranging from several tens of meters to up to 450 m in thickness (Figs. 1 and 8; see reviews in: An et al., 2014; Liu and Ding, 1998). This loess is composed of silt-sized grains containing predominantly quartz, but also significant amounts of feldspar, mica, a varying carbonate content and minor components of clay-sized phyllosilicates (mostly illite, but also smectite, chlorite, kaolinite and vermiculite) as well as iron oxides (Jeong et al., 2011). The loess is interbedded with reddish paleosols due to weathering and oxidation forming nanoscale hematite and other fine-grained phyllosilicates (Fig. 4 B; Bronger and Heinkele, 1989; Chen et al., 2010; Jeong et al., 2011; Maher, 2016; Rutter et al., 1991; Rutter and Ding, 1993). Pedogenic magnetite is observed in the paleosols as well and is responsible for higher magnetic susceptibilities than in the primary loess and commonly used as a proxy for pedogenesis (Ahmed and Maher, 2018; Maher and Thompson, 1991; Zhou et al., 1990). The detrital carbonate grains in the paleosols are leached and precipitated as root casts or carbonate concretions (Bronger and Heinkele, 1989; Rutter et al., 1991; Rutter and Ding, 1993).

Dating of the Chinese loess records revealed a temporal correlation between the loess-paleosol sequences and the glacial-interglacial cycles of the Quaternary period (Fig. 10; Bloemendal et al., 1995; Ding et al.,

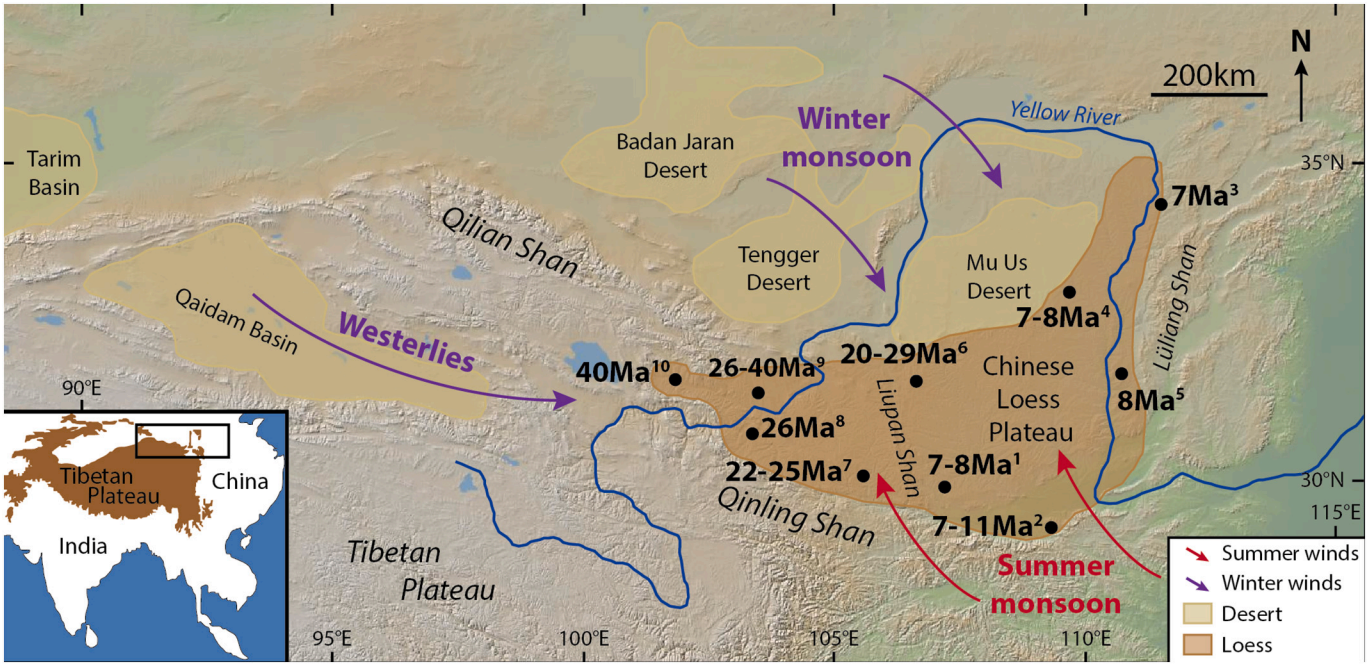

Fig. 9. Map of the Chinese Loess Plateau showing the dominant atmospheric pathways and the various basal ages reported for the onset of loess: 1) central Loess Plateau: Ding et al., 2001; Song et al., 2001; Sun et al., 1997, 1998a, 1998b; 2) southern Loess Plateau: Zheng et al., 1992; Sun et al., 1997; Wang et al., 2014; 3) Baode: Zhu et al. (2008); 4) Jiaxian: Ding et al., 1998b; Qiang et al., 2001; 5) Shilou: Xu et al., 2009; age reinterpreted by Ao et al., 2016; 6) Sikouzi: Jiang and Ding, 2010; age reinterpreted by Wang et al., 2011, 7) Tianshui Basin: Guo et al., 2002; record extended by Qiang et al., 2011; 8) Linxia Basin: Garzione et al., 2005; 9) Lanzhou Basin: Zhang et al., 2014; age reinterpreted by Wang et al., 2016b; 10) Xining Basin: Licht et al., 2014. Modern-day topographic map is from http://www.geomapapp.org.

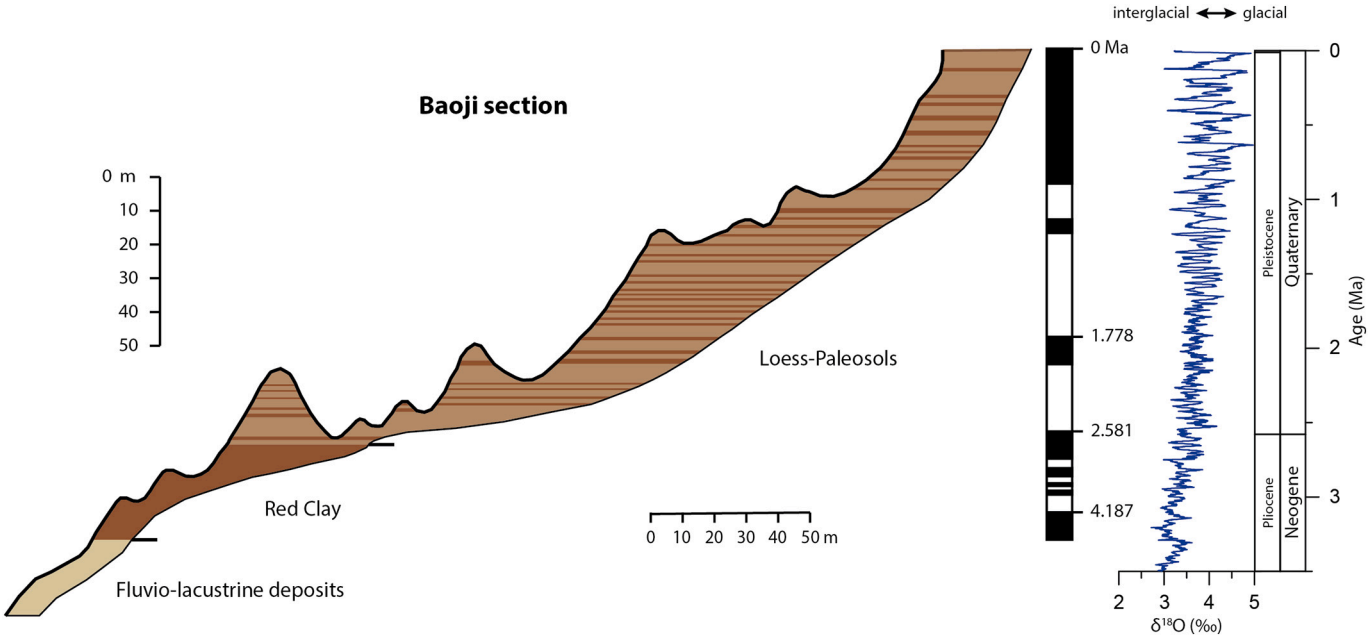

Fig. 10. Stratigraphy at Baoji (central Chinese Loess Plateau) showing fluvio-lacustrine and Red Clay strata underlying the Quaternary loess-paleosol alternations (redrawn from Ding et al., 1994). Magnetostratigraphy is from Evans et al. (1991) with ages recalibrated to the GTS16 (Ogg et al., 2016). Benthic foraminifera $\delta^{18}O$ are shown on the right (5-point moving average through the compilation of Zachos et al., 2008) to reflect the glacial-interglacial cycles. (For interpretation of the references to colour in this figure legend, the reader is referred to the web version of this article.)

1995; Ding et al., 2002; Heller and Liu, 1984; Kukla et al., 1988). The dustier glacial periods are characterized by higher loess accumulation rates and coarser grain-sizes whereas the interglacials correlate to lower accumulation rates, finer grain-sizes and pedogenesis. In terms of atmospheric circulation (Fig. 9), the glacial periods are thought to be dominated by dust storms linked to the low-level westerlies (Kapp et al., 2011; Pullen et al., 2011) and the northwesterly East Asian winter monsoon transporting silt from the arid inlands of the Asian interior (An et al., 1990; Pye and Zhou, 1989; Roe, 2009; Sun et al., 2001; Sun, 2002). The interglacial periods reflect the predominance of the

southeasterly East Asian summer monsoon bringing moisture and promoting soil formation (An et al., 1990). The interplay between these atmospheric configurations is observed on the Chinese Loess Plateau as a gradient of decreasing grain-size and loess thickness going from the dry winter monsoonal northwest to the wetter summer monsoonal southeast (Ding et al., 1999a, 2005; Porter, 2001). In addition, the deposits are increasingly weathered going from the northwest to the southeast (Jeong et al., 2011).

4.2. *Pre-quaternary "loess"*

The Quaternary loess is underlain by Neogene strata that have been proposed to be formed predominantly by dust deposition as well. These strata are commonly referred to as Red Earth, Red Clay or sometimes Hipparion Red Clay after the eponymous fossils found in these deposits (Fig. 10; Mo and Derbyshire, 1991; Flynn et al., 2011; Kaakinen et al., 2013). However, other than the name suggests, most of these deposits consist of fine silt rather than clay (Ding et al., 1998a; Flynn et al., 2011; Guo et al., 2001; Han et al., 2002; Lu et al., 2001; Shang et al., 2016; Yang and Ding, 2004). The beds have a pronounced reddish colour and the sedimentary structure is massive with occasional sub-horizontal laminations (Ding et al., 1998a; Mo and Derbyshire, 1991).

The Red Clay was originally suggested to be fluvio-lacustrine (Kukla, 1987), however Mo and Derbyshire (1991) noted that the microfabric is different than both alluvial and lacustrine sediments and proposed that the Red Clay is formed by weathering on hillslopes and transported over relatively short distances by creep, rainwash and possibly wind. Subsequent studies showed that the fabric of the Red Clay is characterized by pedogenic features including horizonated clay coatings and accumulations of carbonate nodules (Ding et al., 1998a; Guo et al., 2001; Han et al., 2002). These carbonate concretions form laterally extensive horizons that can be readily identified in the field and are comparable to the Quaternary loess-paleosol alternations (Fig. 11; Guo et al., 2001). Zheng et al. (1992) therefore suggested that these pedogenic variations might reflect a similar climatic origin as loess and subsequent studies interpreted the Red Clay as sequences of stacked paleosols (Ding et al., 1997, 1998a; Guo et al., 2001; Han et al., 2002). It should be noted that these pedogenic features indicate subaerial exposure but not a particular mode of sediment transport.

Liu et al. (1988) observed that the magnetic fabric (anisotropy of magnetic susceptibility) is similar to the overlying Quaternary loess and different than loess reworked by water. Furthermore, the mineral content of the Red Clay consists predominantly of angular quartz grains, feldspars and mica's (Guo et al., 2001) as well as clay minerals including mostly illite and some kaolinite, chlorite and smectite (Han et al., 2002; Wang et al., 2019). The geochemical signature of the major and trace elements as well as rare earth element (REE) abundances are comparable with loess (Ding et al., 1998b; Guo et al., 2001; Han et al., 2002). Because of the similarities in mineral content, geochemistry and the massive sedimentary structure, it has been proposed that the Red Clay is formed by the accumulation of eolian dust that subsequently underwent pedogenesis (Ding et al., 1997, 1998a, 1999b; Guo et al., 2001, 2004; Liu et al., 1988; Zheng et al., 1992). However, as discussed in Section 2.4, none these features are not diagnostic for eolian transport alone and may reflect alluvial mudflat deposition as well.

This is corroborated by the numerous fluvial sandstone and gravel beds that are observed to interbed the Red Clay especially in the Miocene strata and contain important localities for mammal fossils (Mo and Derbyshire, 1991; Flynn et al., 2011). In the central Chinese Loess Plateau, east of the Liupan Shan, these sandstone beds are increasing towards the base where they conformably or unconformably overlie Miocene fluvio-lacustrine sand- and siltstones (Fig. 10; Guo et al., 2001; Kaakinen and Lunkka, 2003; Qiang et al., 2001; Sun et al., 1997, 1998a, 1998b; Wang et al., 2014; Zhu et al., 2008) or older sedimentary strata (An et al., 1999; Jiang and Ding, 2010; Song et al., 2001; Xu et al., 2009). Furthermore, there are notable differences between the Red Clay and the Quaternary loess. The accumulation rates in the Red Clay based on magnetostratigraphy are ~3 cm/kyr, which is lower compared to the ~6 cm/kyr in loess and ~ 4 cm/kyr in paleosols (Ding et al., 1998b; Sun et al., 1998a, 1998b). In addition, the grain-size is finer with median grain-sizes of ~5–15 μm and the grain-size distributions are more symmetric compared to the loess which has a median grain-size of ~20–50 μm and a distinct tail of finer grain-sizes (Ding et al., 1998a; Guo et al., 2001; Han et al., 2002; Lu et al., 2001; Shang et al., 2016; Yang and Ding, 2004).

Several hypotheses have been proposed to explain these differences. One of these includes more intense pedogenesis because the grain-size distributions of the Red Clay strata are similar to the Quaternary paleosols (Ding et al., 1999a, 1999b; Guo et al., 2001; Han et al., 2002). Sun et al. (2006) attempted to remove this pedogenic overprint by chemically isolating the quartz grains, which are more stable and unaffected by pedogenesis. Grain-size analysis of this quartz fraction revealed that the grain-size distributions are identical to the primary loess with a coarser median grain-size at ~10–50 μm. They therefore suggested that the coarse component in the Red Clay is derived from winter monsoonal dust storms similar to the Quaternary but more strongly overprinted by

Fig. 11. Picture of the Mio-Pliocene Red Clay at the Shilou section in the eastern Chinese Loess Plateau (photograph courtesy of Hong Ao). (For interpretation of the references to colour in this figure legend, the reader is referred to the web version of this article.)

pedogenesis due to the warmer and possibly wetter climate of the Miocene and Pliocene epochs (Ding et al., 1997, 1998a; Guo et al., 2004; Han et al., 2002; Lu et al., 2001; Miao et al., 2004; Sun et al., 2006; Yang and Ding, 2004). Lower accumulation rates during the Mio-Pliocene would have promoted pedogenesis and thereby enhanced the fine-grained components (Han et al., 2002; Sun et al., 2006). Alternatively, it has been suggested that the fine-grained material in the Red Clay is derived from the upper-level westerly jet stream which could have been the dominant dust transporter during the Neogene (Ding et al., 2000; Vandenberghe et al., 2006; Li et al., 2020). Based on the recent provenance studies indicating significant sediment contributions from local mountain-ranges (Liu et al., 2019; Nie et al., 2014; Shang et al., 2016; Zhang et al., 2018) and fluvial strata interbedding some of the Red Clay sections (Mo and Derbyshire, 1991; Flynn et al., 2011), we propose that mixed alluvial/eolian deposition in mudflat systems should be considered as well and may explain the fine-grained components observed in the Red Clay thereby reflecting a terrestrial mudflat as described in Section 2.3.

Another distinctly different feature of the Red Clay is the magnetic susceptibility, which is less than half of the susceptibility measured in the overlying loess-paleosols (Ding et al., 1997; Hao et al., 2008; Liu et al., 2003). This suggests a reduction in soil-formed magnetite, even though the pedogenic microfabrics in the Red Clay are more prominent (Ding et al., 1999b; Liu et al., 2003). The reason for these lower magnetic susceptibilities remains debated but possibilities include different soil conditions resulting in the dissolution and oxidation of iron oxides in the Red Clay or a shift in provenance of the primary minerals (Ding et al., 1999b; Liu et al., 2003; Nie et al., 2016; Yang and Ding, 2010). Several provenance studies using a variety of tools such as isotopic signatures have indeed reported a change between the Red Clay and the overlying Quaternary Loess (Li et al., 2020; Nie et al., 2014, 2018; Sun, 2005: Sun and Zhu, 2010; Sun et al., 2020; Yan et al., 2017). However, other studies do not find such a provenance shift (Bird et al., 2015; Peng et al., 2016; Wang et al., 2007) and argue that the isotopic variation is due to the higher degree of chemical weathering in the Red Clay (Bird et al., 2020). An alternative explanation for these inconsistencies is that the provenance signal of the Red Clay may be spatially heterogeneous (Sun et al., 2020) possibly due to significant local contributions.

Older records have been identified as loess in the western part of the Chinese Loess Plateau, west of the Liupan Shan (Fig. 9). Guo et al. (2002) identified massive siltstones showing laterally extensive paleosols near Qinan spanning from 22 to 6.2 Ma based on magneto- and biostratigraphy. This record was subsequently extended with a drill-core to cover the late Oligocene with a basal age of 25 Ma (Qiang et al., 2011). Evidence used to argue for an eolian origin of these strata includes grain-size distributions and geochemical properties, which are similar to the loess (Guo et al., 2002, 2008; Hao and Guo, 2004; Liu et al., 2006; Qiang et al., 2011; Qiao et al., 2006). Furthermore, the quartz grains have an angular shape and show conchoidal fractures which may indicate eolian transport (Liu et al., 2006) and terrestrial land snail fossils similar to those found in the Quaternary loess have been identified in the Miocene siltstones (Li et al., 2006a). However, as discussed above, none of these features are diagnostic of eolian transport and more recent sedimentological, stratigraphic and provenance studies argue for predominantly alluvial deposition instead (Alonso-Zarza et al., 2009, 2010; Liu et al., 2019).

Subsequent studies have identified eolian dust, often along with other alluvial components, in even older Paleogene deposits spanning the western Chinese Loess Plateau (Fig. 9). Jiang and Ding (2010) use grain-size distributions and REE patterns to identify dust in the Sikouzi section spanning from ~0.1 to ~20 Ma based on magnetostratigraphy. However, the age of this section was subsequently reinterpreted to cover ~0.5 to ~29 Ma based on magneto- and biostratigraphy (Wang et al., 2011). The siltstones in the Linxia Basin with a basal age of ~26 Ma are interpreted as dust based on the provenance signals (Nd and REE) and the low accumulation rates in the basin, which are comparable to the Red Clay and Quaternary loess (Garzione et al., 2005). Zhang et al. (2014) identified a dominant dust component along with alluvial contributions in the grain-size record of the Lanzhou Basin after ~26 Ma, but a subsequent magnetostratigraphic study reinterpreted this age to ~40 Ma (Wang et al., 2016b). Similarly, an eolian dust component is identified in the mudflat deposits of the Xining Basin after ~40 Ma based on quartz surface morphologies and the provenance signal in detrital zircons (Licht et al., 2014, 2016b).

We suggest that the Red Clay and similar massive terrestrial siltstones are different than the Quaternary loess and more adequately reflect a terrestrial mudflat instead of being entirely composed of eolian dust. This is corroborated by the abundance of closed geomorphic basins throughout Central Asia (Carroll et al., 2010), which would have promoted the development of low-relief mudflats surrounded by active mountain ranges. Although not loess-like, these mudflat deposits provide invaluable terrestrial records of pedogenesis and other paleoclimate proxies for reconstructing the monsoonal evolution in the past. Furthermore, both extrabasinal and intrabasinal dust components may be tracked and used to reconstruct paleoenvironmental conditions. An increase in extrabasinal dust may reflect more dust production and aridification of distal source areas or an intensification of large-scale atmospheric dust transport, whereas intrabasinal dust may indicate local aridity in the basin.

The geological record of the Chinese Loess Plateau is unique because it records the transition between the Red Clay strata and the overlying Quaternary loess, and therefore from a mudflat environment to predominantly dust deposition. This transition is conformable in most locations showing a gradual shift to more loess-like beds (Ding et al., 1997; Kukla, 1987; Yang and Ding, 2010) associated with a ~2- to 3-fold increase in accumulation rate (Ding et al., 1997; Lu et al., 2010). The mudflat-loess transition could therefore reflect a strengthening of the dust storms or an increase in dust production upwind which would have resulted in more dust accumulation and overwhelmed local mudflat deposition. Local environmental shifts on the Loess Plateau could have promoted the efficiency of dust trapping by creating wetted surfaces or increasing the vegetation cover. Magnetostratigraphic studies have dated the Red Clay to loess transition at ~2.8–2.6 Ma, coeval with the Plio-Pleistocene boundary and the onset of Northern Hemisphere glaciation (Fig. 10; Ding et al., 1997; Han et al., 2002; Yang and Ding, 2010; Guo et al., 2020). This confirms the tight coupling between glacial climate and dust accumulation on the Loess Plateau (An et al., 1999; Ding et al., 1997, 2000).

5. Conclusion

Terrestrial dust deposits are well-known from the Quaternary period as bodies of loess draping the underlying topography, but increasingly difficult to recognize in older geological records due to a lack of diagnostic eolian features. Yet numerous siltstones have been interpreted as loessites being formed almost entirely by windblown dust. However, these interpretations are often based on ambiguous criteria, such as massive sedimentary structures, uniform grain-size distributions and angular-shaped quartz grains. Here, we show that such features are not exclusively windblown and may occur as well by alluvial deposition on low-gradient terrestrial mudflats. Such a depositional setting may better explain the provenance signatures of local mountain ranges and the fluvial sandstones observed to interbed supposed loessites.

Eolian dust may settle and accumulate on these mudflats along with other alluvial components and can be reliably quantified in sedimentary records by: 1) quartz surface morphology analysis to identify the modes transport and distinguish eolian from fluvial components, 2) provenance analysis to derive an extrabasinal or local origin, 3) end-member analysis of grain-size and -shape distributions to quantify the various sediment contributions throughout the record, 4) basin-scale analyses to remove local sedimentary features. Acknowledging and unmixing the various eolian and alluvial components in the record will enable a more

reliable and robust estimation of dust in the geological record. This would have important implications for paleoclimate reconstructions and constraints on dust fluxes in the past.

The geological record of the Chinese Loess Plateau is continuous throughout the Neogene and reveals a marked shift from Red Clay strata, interpreted to have formed on a terrestrial mudflat by both alluvial and eolian deposition, to loess, composed almost entirely of windblown dust. The Red Clay-loess transition occurs at the boundary to the Quaternary period and is coeval with the onset of Northern Hemisphere glaciation which may have promoted dust production, mobilization and/or transport (e.g. Ding et al., 1997). This climatic shift would have overwhelmed local mudflat deposition on the Chinese Loess Plateau as evidenced by the abrupt increase in sedimentation rate (e.g. Ding et al., 1997; Lu et al., 2010). This suggests that loess deposits in the geological record may be found only during periods with extensive glaciation such as the Quaternary. Alternatively, exclusively windblown dust deposits may occur during the pre-Quaternary as well but are likely difficult to preserve due to the draping nature of loess bodies on the pre-existing landscape. Over longer geological timescales these loess bodies would be reworked as is occurring today on the Chinese Loess Plateau (Kapp et al., 2015; Licht et al., 2016a, 2016b) before being preserved in the low-lying basins thereby biasing the geological record towards alluvial mudflat deposits. This is exemplified by the Quaternary sediments of the Weihe Basin at the southern margin of the Chinese Loess Plateau which contain predominantly of fluvio-lacustrine deposition of reworked loess and only rare occurrences of primary loess deposition (Rits et al., 2016).

Declaration of Competing Interest

The authors declare that they have no known competing financial interests or personal relationships that could have appeared to influence the work reported in this paper.

Acknowledgements

This work was funded by the ERC consolidator grant MAGIC 649081 to GDN. We thank Koen van Toorenenburg and Yuan Shang for providing grain-size data as well as Hong Ao for providing a photograph of the Shilou section. We thank Anu Kaakinen and one anonymous reviewer for their helpful feedback.

References

Ahmed, I.A., Maher, B.A., 2018. Identification and paleoclimatic significance of magnetite nanoparticles in soils. Proc. Natl. Acad. Sci. 115 (8), 1736–1741. https://doi.org/10.1073/pnas.1719186115.

Alonso-Zarza, A.M., Zhao, Z., Song, C.H., Li, J.J., Zhang, J., Martín-Pérez, A., Martín-García, R., Wang, X.X., Zhang, Y., Zhang, M.H., 2009. Mudflat/distal fan and shallow lake sedimentation (upper Vallesian–Turolian) in the Tianshui Basin, Central China: evidence against the late Miocene eolian loess. Sediment. Geol. 222 (1–2), 42–51. https://doi.org/10.1016/j.sedgeo.2009.03.010.

Alonso-Zarza, A.M., Zhao, Z., Song, C.H., Li, J.J., Zhang, J., Martín-Pérez, A., Martín-García, R., Wang, X.X., Zhang, Y., Zhang, M.H., Meléndez, A., 2010. Reply to the comment on "Mudflat/distal fan and shallow lake sedimentation (upper Vallesian–Turolian) in the Tianshui Basin, Central China: evidence against the late Miocene eolian loess" by AM Alonso-Zarza, Z. Zhao, CH Song, JJ Li, J. Zhang, A. Martín-Pérez, R. Martín-García, XX Wang, Y. Zhang and MH Zhang [Sedimentary Geology 222 (2009) 42–51]. Sediment. Geol. 230 (1–2), 90–93. https://doi.org/10.1016/j.sedgeo.2010.06.018.

An, Z., Liu, T., Lu, Y., Porter, S.C., Kukla, G., Wu, X., Hua, Y., 1990. The long-term paleomonsoon variation recorded by the loess-paleosol sequence in central China. Quat. Int. 7, 91–95. https://doi.org/10.1016/1040-6182(90)90042-3.

An, Z., Wang, S., Wu, X., Chen, M., Sun, D., Liu, X., Wang, F., Li, L., Sun, Y., Zhou, W., Zhou, J., Liu, X., Lu, H., Zhang, Y., Dong, G., Qiang, X., 1999. Eolian evidence from the Chinese Loess Plateau: the onset of the late Cenozoic Great Glaciation in the Northern Hemisphere and Qinghai-Xizang Plateau uplift forcing. Sci. China Ser. D Earth Sci. 42 (3), 258. https://doi.org/10.1007/BF02878963.

An, Z., Kutzbach, J.E., Prell, W.L., Porter, S.C., 2001. Evolution of Asian monsoons and phased uplift of the Himalaya–Tibetan plateau since Late Miocene times. Nature 411 (6833), 62. https://doi.org/10.1038/35075035.

An, Z., Sun, Y., Zhou, W., Liu, W., Qiang, X., Wang, X., Xian, F., Cheng, P., Burr, G.S., 2014. Chinese loess and the East Asian monsoon. In: Late Cenozoic Climate Change in Asia. Springer, Dordrecht, pp. 23–143.

Ao, H., Roberts, A.P., Dekkers, M.J., Liu, X., Rohling, E.J., Shi, Z., An, Z., Zhao, X., 2016. Late Miocene–Pliocene Asian monsoon intensification linked to Antarctic ice-sheet growth. Earth Planet. Sci. Lett. 444, 75–87. https://doi.org/10.1016/j.epsl.2016.03.028.

Assallay, A.M., Rogers, C.D.F., Smalley, I.J., Jefferson, I.F., 1998. Silt: 2–62 μm, 9–4φ. Earth Sci. Rev. 45 (1–2), 61–88. https://doi.org/10.1016/S0012-8252(98)00035-X.

Begét, J.E., Keskinen, M., Severin, K., 1993. Mineral particles from Asia found in volcanic loess on the island of Hawaii. Sediment. Geol. 84 (1–4), 189–197. https://doi.org/10.1016/0037-0738(93)90055-A.

Bellosi, E.S., 2010. Physical Stratigraphy of the Sarmiento Formation (Middle Eocene–Lower Miocene) at Gran Barranca, Central Patagonia. The Paleontology of Gran Barranca. Cambridge University, New York, pp. 19–31.

Bird, A., Stevens, T., Rittner, M., Vermeesch, P., Carter, A., Andò, S., Garzanti, E., Lu, H., Nie, J., Zeng, L., Zhang, H., Xu, Z., 2015. Quaternary dust source variation across the Chinese Loess Plateau. Palaeogeogr. Palaeoclimatol. Palaeoecol. 435, 254–264. https://doi.org/10.1016/j.palaeo.2015.06.024.

Bird, A., Millar, I., Rodenburg, T., Stevens, T., Rittner, M., Vermeesch, P., Lu, H., 2020. A constant Chinese Loess Plateau dust source since the late Miocene. Quat. Sci. Rev. 227, 106042. https://doi.org/10.1016/j.quascirev.2019.106042.

Bloemendal, J., Liu, X.M., Rolph, T.C., 1995. Correlation of the magnetic susceptibility stratigraphy of Chinese loess and the marine oxygen isotope record: chronological and palaeoclimatic implications. Earth Planet. Sci. Lett. 131 (3–4), 371–380. https://doi.org/10.1016/0012-821X(95)00016-6.

Blott, S.J., Pye, K., 2001. GRADISTAT: a grain size distribution and statistics package for the analysis of unconsolidated sediments. Earth Surf. Process. Landf. 26 (11), 1237–1248. https://doi.org/10.1002/esp.261.

Borradaile, G.J., Henry, B., 1997. Tectonic applications of magnetic susceptibility and its anisotropy. Earth Sci. Rev. 42 (1–2), 49–93. https://doi.org/10.1016/S0012-8252(96)00044-X.

Bronger, A., Heinkele, T., 1989. Micromorphology and genesis of paleosols in the Luochuan loess section, China: pedostratigraphic and environmental implications. Geoderma 45 (2), 123–143. https://doi.org/10.1016/0016-7061(89)90046-3.

Carrapa, B., DeCelles, P.G., Wang, X., Clementz, M.T., Mancin, N., Stoica, M., Kraatz, B., Meng, J., Abdulov, S., Chen, F., 2015. Tectono-climatic implications of Eocene Paratethys regression in the Tajik basin of Central Asia. Earth Planet. Sci. Lett. 424, 168–178. https://doi.org/10.1016/j.epsl.2015.05.034.

Carroll, A.R., Graham, S.A., Smith, M.E., 2010. Walled sedimentary basins of China. Basin Res. 22 (1), 17–32.

Chen, T., Xie, Q., Xu, H., Chen, J., Ji, J., Lu, H., Balsam, W., 2010. Characteristics and formation mechanism of pedogenic hematite in Quaternary Chinese loess and paleosols. Catena 81 (3), 217–225. https://doi.org/10.1016/j.catena.2010.04.001.

Chen, J., Liu, X., Liu, X., 2019. Sedimentary dynamics and climatic implications of cretaceous loess-like red beds in the Lanzhou basin, Northwest China. J. Asian Earth Sci. 180, 103865. https://doi.org/10.1016/j.jseaes.2019.05.010.

Cheng, F., Hong, H., Bae, C.J., Li, Z., Algeo, T.J., Huang, S., Cheng, L., Fang, Q., 2018. Geochemical and detrital zircon U-Pb geochronological constraints on provenance of the Xiaomei red earth sediments (Bose Basin, Guangxi Province, southern China). Palaeogeogr. Palaeoclimatol. Palaeoecol. 510, 49–62. https://doi.org/10.1016/j.palaeo.2017.08.040.

Costa, P.J.M., Andrade, C., Mahaney, W.C., Da Silva, F.M., Freire, P., Freitas, M.C., Janardo, C., Oliveira, M.A., Silva, T., Lopes, V., 2013. Aeolian microtextures in silica spheres induced in a wind tunnel experiment: comparison with aeolian quartz. Geomorphology 180, 120–129. https://doi.org/10.1016/j.geomorph.2012.09.011.

Crouvi, O., Amit, R., Enzel, Y., Gillespie, A.R., 2010. Active sand seas and the formation of desert loess. Quat. Sci. Rev. 29 (17–18), 2087–2098. https://doi.org/10.1016/j.quascirev.2010.04.026.

Derbyshire, E., Meng, X., Kemp, R.A., 1998. Provenance, transport and characteristics of modern aeolian dust in western Gansu Province, China, and interpretation of the Quaternary loess record. J. Arid Environ. 39 (3), 497–516. https://doi.org/10.1006/jare.1997.0369.

Dietze, E., Dietze, M., 2019. Grain-size distribution unmixing using the R package EMMAgeo. E&G-Quat. Sci. J. 68, 29–46. https://doi.org/10.5194/egqsj-68-29-2019.

Dietze, E., Maussion, F., Ahlborn, M., Diekmann, B., Hartmann, K., Henkel, K., Kasper, T., Lockot, G., Opitz, S., Haberzettl, T., 2014. Sediment transport processes across the Tibetan Plateau inferred from robust grain-size end members in lake sediments. Clim. Past 10 (1), 91–106. https://doi.org/10.5194/cp-10-91-2014.

Ding, Z., Yu, Z., Rutter, N.W., Liu, T., 1994. Towards an orbital time scale for Chinese loess deposits. Quat. Sci. Rev. 13 (1), 39–70. https://doi.org/10.1016/0277-3791(94)90124-4.

Ding, Z., Liu, T., Rutter, N.W., Yu, Z., Guo, Z., Zhu, R., 1995. Ice-volume forcing of East Asian winter monsoon variations in the past 800,000 years. Quat. Res. 44 (2), 149–159. https://doi.org/10.1006/qres.1995.1059.

Ding, Z., Rutter, N.W., Liu, T., 1997. The onset of extensive loess deposition around the G/M boundary in China and its palaeoclimatic implications. Quat. Int. 40, 53–60. https://doi.org/10.1016/S1040-6182(96)00061-4.

Ding, Z.L., Sun, J.M., Liu, T.S., Zhu, R.X., Yang, S.L., Guo, B., 1998a. Wind-blown origin of the Pliocene red clay formation in the central Loess Plateau, China. Earth Planet. Sci. Lett. 161 (1–4), 135–143. https://doi.org/10.1016/S0012-821X(98)00145-9.

Ding, Z.L., Sun, J.M., Yang, S.L., Liu, T.S., 1998b. Preliminary magnetostratigraphy of a thick eolian red clay-loess sequence at Lingtai, the Chinese Loess Plateau. Geophys. Res. Lett. 25 (8), 1225–1228. https://doi.org/10.1029/98GL00836.

Ding, Z., Sun, J., Rutter, N.W., Rokosh, D., Liu, T., 1999a. Changes in sand content of loess deposits along a north–south transect of the Chinese Loess Plateau and the implications for desert variations. Quat. Res. 52 (1), 56–62. https://doi.org/10.1006/qres.1999.2045.

Ding, Z.L., Xiong, S.F., Sun, J.M., Yang, S.L., Gu, Z.Y., Liu, T.S., 1999b. Pedostratigraphy and paleomagnetism of a~ 7.0 Ma eolian loess–red clay sequence at Lingtai, Loess Plateau, north-Central China and the implications for paleomonsoon evolution. Palaeogeogr. Palaeoclimatol. Palaeoecol. 152 (1–2), 49–66. https://doi.org/10.1016/S0031-0182(99)00034-6.

Ding, Z.L., Rutter, N.W., Sun, J.M., Yang, S.L., Liu, T.S., 2000. Re-arrangement of atmospheric circulation at about 2.6 Ma over northern China: evidence from grain size records of loess-palaeosol and red clay sequences. Quat. Sci. Rev. 19 (6), 547–558. https://doi.org/10.1016/S0277-3791(99)00017-7.

Ding, Z.L., Yang, S.L., Hou, S.S., Wang, X., Chen, Z., Liu, T.S., 2001. Magnetostratigraphy and sedimentology of the Jingchuan red clay section and correlation of the Tertiary eolian red clay sediments of the Chinese Loess Plateau. J. Geophys. Res. 106 (B4), 6399–6407. https://doi.org/10.1029/2000JB900445.

Ding, Z.L., Derbyshire, E., Yang, S.L., Yu, Z.W., Xiong, S.F., Liu, T.S., 2002. Stacked 2.6-Ma grain size record from the Chinese loess based on five sections and correlation with the deep-sea δ18O record. Paleoceanography 17 (3), 5–11. https://doi.org/10.1029/2001PA000725.

Ding, Z.L., Derbyshire, E., Yang, S.L., Sun, J.M., Liu, T.S., 2005. Stepwise expansion of desert environment across northern China in the past 3.5 Ma and implications for monsoon evolution. Earth Planet. Sci. Lett. 237 (1–2), 45–55. https://doi.org/10.1016/j.epsl.2005.06.036.

D'Odorico, P., Bhattachan, A., Davis, K.F., Ravi, S., Runyan, C.W., 2013. Global desertification: drivers and feedbacks. Adv. Water Resour. 51, 326–344. https://doi.org/10.1016/j.advwatres.2012.01.013.

Donselaar, M.E., Gozalo, M.C., Moyano, S., 2013. Avulsion processes at the terminus of low-gradient semi-arid fluvial systems: lessons from the Rio Colorado, Altiplano endorheic basin, Bolivia. Sediment. Geol. 283, 1–14. https://doi.org/10.1016/j.sedgeo.2012.10.007.

Durand, M., Bourquin, S., 2013. Criteria for the identification of ventifacts in the geological record: a review and new insights. Compt. Rendus Geosci. 345 (3), 111–125. https://doi.org/10.1016/j.crte.2013.02.004.

Edwards, M.B., 1979. Late Precambrian glacial loessites from north Norway and Svalbard. J. Sediment. Res. 49 (1), 85–91. https://doi.org/10.1306/212F76C6-2B24-11D7-8648000102C1865D.

Evans, M.E., Wang, Y., Rutter, N., Ding, Z., 1991. Preliminary magnetostratigraphy of the red clay underlying the loess sequence at Baoji, China. Geophys. Res. Lett. 18 (8), 1409–1412. https://doi.org/10.1029/91GL01800.

Fan, M., Feng, R., Geissman, J.W., Poulsen, C.J., 2020. Late Paleogene emergence of a North American loess plateau. Geology 48 (3), 273–277. https://doi.org/10.1130/G47102.1.

Flynn, L.J., Tao, D., Yang, W., Guangpu, X., Sukuan, H., Libo, P., Yongqing, M., 2011. Observations on the Hipparion Red Clays of the Loess Plateau. Vertebrata PalAsiatica. http://nrs.harvard.edu/urn-3:HUL.InstRepos:34325479.

Gallet, S., Jahn, B., Van Vliet Lanoë, B., Dia, A., Rosello, E., 1998. Loess geochemistry and its application for particle origin and composition of the upper continental crust. Earth Planet. Sci. Lett. 156, 157–172. https://doi.org/10.1016/S0012-821X(97)00218-5.

Garzione, C.N., Ikari, M.J., Basu, A.R., 2005. Source of Oligocene to Pliocene sedimentary rocks in the Linxia basin in northeastern Tibet from Nd isotopes: implications for tectonic forcing of climate. GSA Bull. 117 (9–10), 1156–1166. https://doi.org/10.1130/B25743.1.

Goossens, D., 2008. Techniques to measure grain-size distributions of loamy sediments: a comparative study of ten instruments for wet analysis. Sedimentology 55 (1), 65–96. https://doi.org/10.1111/j.1365-3091.2007.00893.x.

Guo, Z.T., Peng, S.Z., Hao, Q.Z., Biscaye, P.E., Liu, T.S., 2001. Origin of the Miocene–Pliocene red-earth formation at Xifeng in Northern China and implications for paleoenvironments. Palaeogeogr. Palaeoclimatol. Palaeoecol. 170 (1–2), 11–26. https://doi.org/10.1016/S0031-0182(01)00235-8.

Guo, Z.T., Ruddiman, W.F., Hao, Q.Z., Wu, H.B., Qiao, Y.S., Zhu, R.X., Peng, S.Z., Wei, J. J., Yuan, B.Y., Liu, T.S., 2002. Onset of Asian desertification by 22 Myr ago inferred from loess deposits in China. Nature 416 (6877), 159. https://doi.org/10.1038/416159a.

Guo, Z., Peng, S., Hao, Q., Biscaye, P.E., An, Z., Liu, T., 2004. Late Miocene–Pliocene development of Asian aridification as recorded in the Red-Earth Formation in northern China. Glob. Planet. Chang. 41 (3–4), 135–145. https://doi.org/10.1016/j.gloplacha.2004.01.002.

Guo, Z.T., Sun, B., Zhang, Z.S., Peng, S.Z., Xiao, G.Q., Ge, J.Y., Hao, Q.Z., Qiao, Y.S., Liang, M.Y., Liu, J.F., Yin, Q.Z., Wei, J.J., 2008. A major reorganization of Asian climate by the early Miocene. Clim. Past 4 (3).

Guo, Z.T., Ge, J.Y., Xiao, G.Q., Hao, Q.Z., Wu, H.B., Zhan, T., Liu, L., Qin, L., Zeng, F.M., Yuan, B.Y., 2010. Comment on "Mudflat/distal fan and shallow lake sedimentation (upper Vallesian–Turolian) in the Tianshui Basin, Central China: Evidence against the late Miocene eolian loess" by AM Alonso-Zarza, Z. Zhao, CH Song, JJ Li, J. Zhang, A. Martín-Pérez, R. Martín-García, XX Wang, Y. Zhang and MH Zhang [Sedimentary Geology 222 (2009) 42–51]. Sediment. Geol. 230 (1–2), 86–89. https://doi.org/10.1016/j.sedgeo.2010.06.019.

Guo, B., Peng, T., Yu, H., Hui, Z., Ma, Z., Li, X., Feng, Z., Liu, J., Liu, S., Zhang, J., Ye, X., Song, C., Li, J., 2020. Magnetostratigraphy and palaeoclimatic significance of the late pliocene red clay-quaternary loess sequence in the Lanzhou Basin, Western Chinese Loess Plateau. Geophys. Res. Lett. 47 (3) https://doi.org/10.1029/2019GL086556 e2019GL086556.

Hajek, E.A., Straub, K.M., 2017. Autogenic sedimentation in clastic stratigraphy. Annu. Rev. Earth Planet. Sci. 45, 681–709.

Han, J., Fyfe, W.S., Gu, Z., 2002. Assessment of the palaeoclimate during 3.0–2.6 Ma registered by transition of Red Clay to loess–palaeosol sequence in central North China. Palaeogeogr. Palaeoclimatol. Palaeoecol. 185 (3–4), 355–368. https://doi.org/10.1016/S0031-0182(02)00382-6.

Hao, Q., Guo, Z., 2004. Magnetostratigraphy of a late Miocene-Pliocene loess-soil sequence in the western Loess Plateau in China. Geophys. Res. Lett. 31 (9) https://doi.org/10.1029/2003GL019392.

Hao, Q., Oldfield, F., Bloemendal, J., Guo, Z., 2008. The magnetic properties of loess and paleosol samples from the Chinese Loess Plateau spanning the last 22 million years. Palaeogeogr. Palaeoclimatol. Palaeoecol. 260 (3–4), 389–404. https://doi.org/10.1016/j.palaeo.2007.11.010.

Hardie, L.A., Smoot, J.P., Eugster, H.P., 1978. Saline lakes and their deposits: a sedimentological approach. In: Modern and Ancient Lake Sediments, Vol. 2. Blackwell Oxford, pp. 7–41. https://doi.org/10.1002/9781444303698.ch2.

Hays, J.D., Imbrie, J., Shackleton, N.J., 1976. Variations in the Earth's orbit: pacemaker of the ice ages. Science 194 (4270), 1121–1132.

Heavens, N.G., Shields, C.A., Mahowald, N.M., 2012. A paleogeographic approach to aerosol prescription in simulations of deep time climate. J. Adv. Model. Earth Syst. 4 (4) https://doi.org/10.1029/2012MS000166.

Heller, F., Liu, T., 1984. Magnetism of Chinese loess deposits. Geophys. J. Int. 77 (1), 125–141. https://doi.org/10.1111/j.1365-246X.1984.tb01928.x.

Hunter, R.E., 1977. Basic types of stratification in small eolian dunes. Sedimentology 24 (3), 361–387. https://doi.org/10.1111/j.1365-3091.1977.tb00128.x.

Jefferson, I., Rosenbaum, M., Smalley, I., 2002. Mercia Mudstone as a Triassic aeolian desert sediment. Mercian Geol. 15 (3), 157–162.

Jeong, G.Y., Hillier, S., Kemp, R.A., 2011. Changes in mineralogy of loess–paleosol sections across the Chinese Loess Plateau. Quat. Res. 75 (1), 245–255. https://doi.org/10.1016/j.yqres.2010.09.001.

Jiang, H., Ding, Z., 2010. Eolian grain-size signature of the Sikouzi lacustrine sediments (Chinese Loess Plateau): implications for Neogene evolution of the East Asian winter monsoon. Bulletin 122 (5–6), 843–854. https://doi.org/10.1130/B26583.1.

Jickells, T.D., An, Z.S., Andersen, K.K., Baker, A.R., Bergametti, G., Brooks, N., Cao, J.J., Boyd, P.W., Duce, R.A., Hunter, K.A., Kawahata, H., Kubilay, N., la Roche, J., Liss, P. S., Mahowald, N., Prospero, J.M., Ridgwell, A.J., Tegen, I., Torres, R., 2005. Global iron connections between desert dust, ocean biogeochemistry, and climate. Science 308 (5718), 67–71.

Johnson, S.Y., 1989. Significance of loessite in the Maroon Formation (middle Pennsylvanian to lower Permian), Eagle basin, Northwest Colorado. J. Sediment. Res. 59 (5), 782–791. https://doi.org/10.1306/212F9070-2B24-11D7-8648000102C1865D.

Kaakinen, A., Lunkka, J.P., 2003. Sedimentation of the Late Miocene Bahe Formation and its implications for stable environments adjacent to Qinling mountains in Shaanxi, China. J. Asian Earth Sci. 22 (1), 67–78. https://doi.org/10.1016/S1367-9120(03)00044-0.

Kaakinen, A., Passey, B.H., Zhang, Z.Q., Liu, L., Pesonen, L.J., Fortelius, M., 2013. Stratigraphy and Paleoecology of the Classical Dragon Bone Localities of Baode County, Shanxi Province. Fossil Mammals of Asia: Neogene Biostratigraphy and Chronology. Columbia University Press, New York, pp. 203–217.

Kapp, P., Pelletier, J.D., Rohrmann, A., Heermance, R., Russell, J., Ding, L., 2011. Wind erosion in the Qaidam basin, central Asia: implications for tectonics, paleoclimate, and the source of the Loess Plateau. GSA Today 21 (4/5), 4–10. https://doi.org/10.1130/GSATG99A.1.

Kapp, P., Pullen, A., Pelletier, J.D., Russell, J., Goodman, P., Cai, F., 2015. From dust to dust: quaternary wind erosion of the Mu Us Desert and Loess Plateau, China. Geology 43 (9), 835–838. https://doi.org/10.1130/G36724.1.

Keiser, L.J., Soreghan, G.S., Kowalewski, M., 2015. Use of quartz microtextural analysis to assess possible proglacial deposition for the Pennsylvanian–Permian Cutler Formation (Colorado, USA). J. Sediment. Res. 85 (11), 1310–1322. https://doi.org/10.2110/jsr.2015.81.

Knippertz, P., Stuut, J.B.W., 2014. Mineral Dust, 10. Springer Dordrecht Heidelberg, New York London, pp. 978–994.

Krinsley, D.H., McCoy, F.W., 1977. Significance and origin of surface textures on broken sand grains in deep-sea sediments. Sedimentology 24 (6), 857–862. https://doi.org/10.1111/j.1365-3091.1977.tb01920.x.

Krinsley, D.T., Smalley, I.J., 1973. Shape and nature of small sedimentary quartz particles. Science 180 (4092), 1277–1279. https://doi.org/10.1126/science.180.4092.1277.

Krinsley, D., Takahashi, T., 1962. Applications of electron microscopy to geology. Trans. New York Acad. Sci. 25 (1 Series II), 3–22. https://doi.org/10.1111/j.2164-0947.1962.tb03509.x.

Krinsley, D., Trusty, P., 1985. Environmental Interpretation of Quartz Grain Surface Textures. In: Provenance of Arenites. Springer, Dordrecht, pp. 213–229. https://doi.org/10.1007/978-94-017-2809-6_10.

Kukla, G., 1987. Loess stratigraphy in central China. Quat. Sci. Rev. 6 (3–4), 191–219. https://doi.org/10.1016/0277-3791(87)90004-7.

Kukla, G., Heller, F., Ming, L.X., Chun, X.T., Sheng, L.T., Sheng, A.Z., 1988. Pleistocene climates in China dated by magnetic susceptibility. Geology 16 (9), 811–814. https://doi.org/10.1130/0091-7613(1988)016<0811:PCICDB>2.3.CO;2.

Large, D.J., Marshall, C., 2015. Use of carbon accumulation rates to estimate the duration of coal seams and the influence of atmospheric dust deposition on coal composition. Geol. Soc. Lond., Spec. Publ. 404 (1), 303–315. https://doi.org/10.1144/SP404.15.

Lee, L.A., Reddington, C.L., Carslaw, K.S., 2016. On the relationship between aerosol model uncertainty and radiative forcing uncertainty. Proc. Natl. Acad. Sci. 113 (21), 5820–5827. https://doi.org/10.1073/pnas.1507050113.

Li, F., Wu, N., Pei, Y., Hao, Q., Rousseau, D.D., 2006a. Wind-blown origin of Dongwan late Miocene–Pliocene dust sequence documented by land snail record in western Chinese Loess Plateau. Geology 34 (5), 405–408. https://doi.org/10.1130/G22232.1.

Li, J., Zhang, J., Song, C., Zhao, Z., Zhang, Y., Wang, X., Zhang, J., Cui, Q., 2006b. Miocene Bahean stratigraphy in the Longzhong Basin, northern central China and its implications in environmental change. Sci. China Ser. D Earth Sci. 49 (12), 1270–1279. https://doi.org/10.1007/s11430-006-2057-y.

Li, J.X., Yue, L.P., Roberts, A.P., Hirt, A.M., Pan, F., Guo, L., Xu, Y., Xi, R.G., Guo, L., Qiang, X.K., Gai, C.C., Jiang, Z.X., Sun, Z.M., Liu, Q.S., 2018. Global cooling and enhanced Eocene Asian mid-latitude interior aridity. Nat. Commun. 9 (1), 3026. https://doi.org/10.1038/s41467-018-05415-x.

Li, Y., Shi, W., Aydin, A., Beroya-Eitner, M.A., Gao, G., 2020. Loess genesis and worldwide distribution. Earth Sci. Rev. 102947 https://doi.org/10.1016/j.earscirev.2019.102947.

Licht, A., Van Cappelle, M., Abels, H.A., Ladant, J.B., Trabucho-Alexandre, J., France-Lanord, C., Donnadieu, Y., Vandenberghe, J., Rigaudier, T., Lécuyer, C., Terry Jr., D., Adriaens, R., Boura, A., Guo, Z., Soe, Aung Naing, Quade, J., Dupont-Nivet, G., Jaeger, J.-J., 2014. Asian monsoons in a late Eocene greenhouse world. Nature 513 (7519), 501–506. https://doi.org/10.1038/nature13704.

Licht, A., Pullen, A., Kapp, P., Abell, J., Giesler, N., 2016a. Eolian cannibalism: reworked loess and fluvial sediment as the main sources of the Chinese Loess Plateau. Bulletin 128 (5–6), 944–956. https://doi.org/10.1130/B31375.1.

Licht, A., Dupont-Nivet, G., Pullen, A., Kapp, P., Abels, H.A., Lai, Z., Guo, Z., Abell, J., Giesler, D., 2016b. Resilience of the Asian atmospheric circulation shown by Paleogene dust provenance. Nat. Commun. 7, 12390. https://doi.org/10.1038/ncomms12390.

Lisiecki, L.E., Raymo, M.E., 2005. A Pliocene-Pleistocene stack of 57 globally distributed benthic δ18O records. Paleoceanography 20 (1). https://doi.org/10.1029/2004PA001071.

Liu, T., Ding, Z., 1998. Chinese loess and the paleomonsoon. Annu. Rev. Earth Planet. Sci. 26 (1), 111–145. https://doi.org/10.1146/annurev.earth.26.1.111.

Liu, X., Xu, T., Liu, T., 1988. The Chinese loess in Xifeng, II. A study of anisotropy of magnetic susceptibility of loess from Xifeng. Geophys. J. Int. 92 (2), 349–353. https://doi.org/10.1111/j.1365-246X.1988.tb01147.x.

Liu, X.M., Rolph, T., An, Z., Hesse, P., 2003. Paleoclimatic significance of magnetic properties on the Red Clay underlying the loess and paleosols in China. Palaeogeogr. Palaeoclimatol. Palaeoecol. 199 (1–2), 153–166. https://doi.org/10.1016/S0031-0182(03)00504-2.

Liu, J., Guo, Z., Qiao, Y., Hao, Q., Yuan, B., 2006. Eolian origin of the Miocene loess-soil sequence at Qin'an, China: evidence of quartz morphology and quartz grain-size. Chin. Sci. Bull. 51 (1), 117–120.

Liu, S., Li, J., Stockli, D.F., Song, C., Guo, B., Stockli, L.D., Ma, Z., Li, X., Peng, T., 2019. Reappraisal of Miocene eolian deposition in Tianshui Basin, China, based on an investigation of stratigraphy and provenance. Geol. Soc. Am. Bull. https://doi.org/10.1130/B32056.1.

Lu, H., Vandenberghe, J., An, Z., 2001. Aeolian origin and palaeoclimatic implications of the 'red clay'(North China) as evidenced by grain-size distribution. J. Quat. Sci. 16 (1), 89–97. https://doi.org/10.1002/1099-1417(200101)16:1<89::AID-JQS578>3.0.CO;2-.

Lu, H., Wang, X., Li, L., 2010. Aeolian sediment evidence that global cooling has driven late Cenozoic stepwise aridification in central Asia. Geol. Soc. Lond., Spec. Publ. 342 (1), 29–44. https://doi.org/10.1144/SP342.4.

Maher, B.A., 2016. Palaeoclimatic records of the loess/palaeosol sequences of the Chinese Loess Plateau. Quat. Sci. Rev. 154, 23–84. https://doi.org/10.1016/j.quascirev.2016.08.004.

Maher, B.A., Thompson, R., 1991. Mineral magnetic record of the Chinese loess and paleosols. Geology 19 (1), 3–6. https://doi.org/10.1130/0091-7613(1991)019<0003:MMROTC>2.3.CO;2.

Marshall, C., Large, D.J., Heavens, N.G., 2016. Coal-derived rates of atmospheric dust deposition during the Permian. Gondwana Res. 31, 20–29. https://doi.org/10.1016/j.gr.2015.10.002.

Martin, J.H., 1990. Glacial-interglacial CO2 change: the iron hypothesis. Paleoceanography 5 (1), 1–13. https://doi.org/10.1029/PA005i001p00001.

Meijer, N., Dupont-Nivet, G., Barbolini, N., Woutersen, A., Rohrmann, A., Zhang, Y., Liu, X. J., Licht, A., Abels, H. A., Hoorn, C., Tjallingii, R., Andermann, C., Dietze, M., Nowaczyk, N. (in review). Loess-like dust appearance at 40 Ma in central China. Paleoceanography and paleoclimatology.

Miao, X., Sun, Y., Lu, H., Mason, J.A., 2004. Spatial pattern of grain size in the Late Pliocene 'Red Clay' deposits (North China) indicates transport by low-level northerly winds. Palaeogeogr. Palaeoclimatol. Palaeoecol. 206 (1–2), 149–155. https://doi.org/10.1016/j.palaeo.2004.01.018.

Mo, D., Derbyshire, E., 1991. The depositional environment of the late Pliocene "red clay", Jing-Le Basin, Shanxi Province, China. Sediment. Geol. 70 (1), 33–40. https://doi.org/10.1016/0037-0738(91)90064-K.

Muhs, D.R., 2013. The geologic records of dust in the Quaternary. Aeolian Res. 9, 3–48. https://doi.org/10.1016/j.aeolia.2012.08.001.

Muhs, D.R., Bettis, E.A., 2003. Quaternary loess-paleosol sequences as examples of climate-driven sedimentary extremes. In: Special Papers-Geological Society of America, pp. 53–74.

Nie, J., Peng, W., Möller, A., Song, Y., Stockli, D.F., Stevens, T., Horton, B.K., Liu, S., Bird, A., Oalmann, J., Gong, H., Fang, X., 2014. Provenance of the upper Miocene–Pliocene Red Clay deposits of the Chinese loess plateau. Earth Planet. Sci. Lett. 407, 35–47. https://doi.org/10.1016/j.epsl.2014.09.026.

Nie, J., Stevens, T., Rittner, M., Stockli, D., Garzanti, E., Limonta, M., Bird, A., Andò, S., Vermeesch, P., Saylor, J., Lu, H., Breecker, D., Hu, X., Liu, S., Resentini, A., Vezzoli, G., Pen, W., Carter, A., Ji, S., Pan, B., 2015. Loess plateau storage of northeastern Tibetan plateau-derived Yellow River sediment. Nat. Commun. 6 (1), 1–10.

Nie, J., Song, Y., King, J.W., 2016. A review of recent advances in red-clay environmental magnetism and paleoclimate history on the Chinese Loess Plateau. Front. Earth Sci. 4, 27. https://doi.org/10.3389/feart.2016.00027.

Nie, J., Pullen, A., Garzione, C.N., Peng, W., Wang, Z., 2018. Pre-Quaternary decoupling between Asian aridification and high dust accumulation rates. Sci. Adv. 4 (2) https://doi.org/10.1126/sciadv.aao6977 eaao6977.

Nieter, W.M., Krinsley, D.H., 1976. The production and recognition of aeolian features on sand grains by silt abrasion. Sedimentology 23 (5), 713–720. https://doi.org/10.1111/j.1365-3091.1976.tb00104.x.

Nottebaum, V., Stauch, G., Hartmann, K., Zhang, J., Lehmkuhl, F., 2015. Unmixed loess grain size populations along the northern Qilian Shan (China): relationships between geomorphologic, sedimentologic and climatic controls. Quat. Int. 372, 151–166. https://doi.org/10.1016/j.quaint.2014.12.071.

Obrist-Farner, J., Yang, W., 2016. Implications of loess and fluvial deposits on paleoclimatic conditions during an icehouse–hothouse transition, Capitanian upper Quanzijie low-order cycle, Bogda Mountains, NW China. Palaeogeogr. Palaeoclimatol. Palaeoecol. 441, 959–981. https://doi.org/10.1016/j.palaeo.2015.10.041.

Ogg, J.G., Ogg, G., Gradstein, F.M., 2016. A concise Geologic Time Scale: 2016. Elsevier.

Paterson, G.A., Heslop, D., 2015. New methods for unmixing sediment grain size data. Geochem. Geophys. Geosyst. 16 (12), 4494–4506. https://doi.org/10.1002/2015GC006070.

Pécsi, M., 1990. Loess is not just the accumulation of dust. Quat. Int. 7, 1–21. https://doi.org/10.1016/1040-6182(90)90034-2.

Peng, W., Wang, Z., Song, Y., Pfaff, K., Luo, Z., Nie, J., Chen, W., 2016. A comparison of heavy mineral assemblage between the loess and the Red Clay sequences on the Chinese Loess Plateau. Aeolian Res. 21, 87–91. https://doi.org/10.1016/j.aeolia.2016.02.004.

Porter, S.C., 2001. Chinese loess record of monsoon climate during the last glacial–interglacial cycle. Earth Sci. Rev. 54 (1–3), 115–128. https://doi.org/10.1016/S0012-8252(01)00043-5.

Potter, P.E., Maynard, J.B., Depetris, P.J., 2005. Mud and Mudstones: Introduction and Overview. Springer Science & Business Media.

Prins, M.A., Vriend, M., Nugteren, G., Vandenberghe, J., Lu, H., Zheng, H., Weltje, G.J., 2007. Late Quaternary aeolian dust input variability on the Chinese Loess Plateau: inferences from unmixing of loess grain-size records. Quat. Sci. Rev. 26 (1–2), 230–242. https://doi.org/10.1016/j.quascirev.2006.07.002.

Pullen, A., Kapp, P., McCallister, A.T., Chang, H., Gehrels, G.E., Garzione, C.N., Heermance, R.V., Ding, L., 2011. Qaidam Basin and northern Tibetan Plateau as dust sources for the Chinese Loess Plateau and paleoclimatic implications. Geology 39 (11), 1031–1034. https://doi.org/10.1130/G32296.1.

Pye, K., 1987. Aeolian Dust and Dust Deposits. Academic Press, San Diego, CA (334 pp.).

Pye, K., 1995. The nature, origin and accumulation of loess. Quat. Sci. Rev. 14 (7–8), 653–667. https://doi.org/10.1016/0277-3791(95)00047-X.

Pye, K., Zhou, L.P., 1989. Late Pleistocene and Holocene aeolian dust deposition in north China and the northwest Pacific Ocean. Palaeogeogr. Palaeoclimatol. Palaeoecol. 73 (1–2), 11–23. https://doi.org/10.1016/0031-0182(89)90041-2.

Qiang, X.K., Li, Z.X., Powell, C.M., Zheng, H.B., 2001. Magnetostratigraphic record of the Late Miocene onset of the East Asian monsoon, and Pliocene uplift of northern Tibet. Earth Planet. Sci. Lett. 187 (1–2), 83–93. https://doi.org/10.1016/S0012-821X(01)00281-3.

Qiang, X., An, Z., Song, Y., Chang, H., Sun, Y., Liu, W., Ao, H., Dong, J., Fu, C., Wu, F., Lu, F., Cia, Y., Zhou, W., Cao, J., Xu, X., Ai, L., 2011. New eolian red clay sequence on the western Chinese Loess Plateau linked to onset of Asian desertification about 25 Ma ago. Sci. China Earth Sci. 54 (1), 136–144. https://doi.org/10.1007/s11430-010-4126-5.

Qiao, Y., Guo, Z., Hao, Q., Yin, Q., Yuan, B., Liu, T., 2006. Grain-size features of a Miocene loess-soil sequence at Qinan: Implications on its origin. Sci. China Ser. D 49 (7), 731–738. https://doi.org/10.1007/s11430-006-0731-8.

Richthofen, B.F., 1882. II.—On the mode of origin of the loess. Geol. Mag. 9 (7), 293–305. https://doi.org/10.1017/S001675680017164X.

Říha, K., Křupka, A., Costa, P.J., 2019. Image analysis applied to quartz grain microtextural provenance studies. Comput. Geosci. 125, 98–108. https://doi.org/10.1016/j.cageo.2019.01.007.

Rits, D.S., Prins, M.A., Troelstra, S.R., van Balen, R.T., Zheng, Y., Beets, C.J., Wang, B., Li, X., Zhou, J., Zheng, H., 2016. Facies analysis of the Middle and Late Quaternary sediment infill of the northern Weihe Basin, Central China. J. Quat. Sci. 31 (2), 152–165. https://doi.org/10.1002/jqs.2853.

Roe, G., 2009. On the interpretation of Chinese loess as a paleoclimate indicator. Quat. Res. 71 (2), 150–161. https://doi.org/10.1016/j.yqres.2008.09.004.

Rust, B.R., Nanson, G.C., 1989. Bedload transport of mud as pedogenic aggregates in modern and ancient rivers. Sedimentology 36 (2), 291–306. https://doi.org/10.1111/j.1365-3091.1989.tb00608.x.

Rutter, N., Ding, Z., 1993. Paleoclimates and monsoon variations interpreted from micromorphogenic features of the Baoji paleosols, China. Quat. Sci. Rev. 12 (10), 853–862. https://doi.org/10.1016/0277-3791(93)90024-G.

Rutter, N., Ding, Z., Evans, M.E., Liu, T., 1991. Baoji-type pedostratigraphic section, Loess Plateau, north-central China. Quat. Sci. Rev. 10 (1), 1–22. https://doi.org/10.1016/0277-3791(91)90028-S.

Schwartz, S.E., Andreae, M.O., 1996. Uncertainty in climate change caused by aerosols. Science 272 (5265). https://doi.org/10.1126/science.272.5265.1121, 1121-1121.

Selkin, P.A., Strömberg, C.A., Dunn, R., Kohn, M.J., Carlini, A.A., Davies-Vollum, K.S., Madden, R.H., 2015. Climate, dust, and fire across the Eocene-Oligocene transition, Patagonia. Geology 43 (7), 567–570. https://doi.org/10.1130/G36664.1.

Shang, Y., Beets, C.J., Tang, H., Prins, M.A., Lahaye, Y., van Elsas, R., Sukselainen, L., Kaakinen, A., 2016. Variations in the provenance of the late Neogene Red Clay

deposits in northern China. Earth Planet. Sci. Lett. 439, 88–100. https://doi.org/10.1016/j.epsl.2016.01.031.
Shang, Y., Kaakinen, A., Beets, C.J., Prins, M.A., 2018. Aeolian silt transport processes as fingerprinted by dynamic image analysis of the grain size and shape characteristics of Chinese loess and Red Clay deposits. Sediment. Geol. 375, 36–48. https://doi.org/10.1016/j.sedgeo.2017.12.001.
Smalley, I.J., 1966a. The properties of glacial loess and the formation of loess deposits. J. Sediment. Res. 36 (3), 669–676. https://doi.org/10.1306/74D7153C-2B21-11D7-8648000102C1865D.
Smalley, I.J., 1966b. Formation of quartz sand. Nature 211 (5048), 476–479.
Smalley, I.J., 1972. The interaction of great rivers and large deposits of primary loess. Trans. New York Acad. Sci. 34 (6 Series II), 534–542. https://doi.org/10.1111/j.2164-0947.1972.tb02706.x.
Smalley, I., 1995. Making the material: the formation of silt sized primary mineral particles for loess deposits. Quat. Sci. Rev. 14 (7–8), 645–651. https://doi.org/10.1016/0277-3791(95)00046-1.
Smalley, I.J., Krinsley, D.H., 1978. Loess deposits associated with deserts. Catena 5 (1), 53–66. https://doi.org/10.1016/S0341-8162(78)80006-X.
Smalley, I.J., Vita-Finzi, C., 1968. The formation of fine particles in sandy deserts and the nature of 'desert' loess. J. Sediment. Res. 38 (3), 766–774. https://doi.org/10.1306/74D71A69-2B21-11D7-8648000102C1865D.
Smalley, I.J., Jefferson, I.F., Dijkstra, T.A., Derbyshire, E., 2001. Some major events in the development of the scientific study of loess. Earth Sci. Rev. 54 (1–3), 5–18. https://doi.org/10.1016/S0012-8252(01)00038-1.
Smalley, I., O'Hara-Dhand, K., Wint, J., Machalett, B., Jary, Z., Jefferson, I., 2009. Rivers and loess: the significance of long river transportation in the complex event-sequence approach to loess deposit formation. Quat. Int. 198 (1–2), 7–18. https://doi.org/10.1016/j.quaint.2008.06.009.
Smoot, J.P., Lowenstein, T.K., 1991. Depositional environments of non-marine evaporites. In: Developments in Sedimentology, Vol. 50. Elsevier, pp. 189–347. https://doi.org/10.1016/S0070-4571(08)70261-9.
Smoot, J.P., Olsen, P.E., 1988. Massive mudstones in basin analysis and paleoclimatic interpretation of the Newark Supergroup. In: Developments in Geotectonics, Vol. 22. Elsevier, pp. 249–274. https://doi.org/10.1016/B978-0-444-42903-2.50015-4.
Song, Y., Fang, X., Masayuki, T., Naoto, I., Li, J., An, Z., 2001. Magnetostratigraphy of Late Tertiary sediments from the Chinese Loess Plateau and its paleoclimatic significance. Chin. Sci. Bull. 46 (1), 16–21. https://doi.org/10.1007/BF03187230.
Soreghan, M.J., Soreghan, G.S., Hamilton, M.A., 2002. Paleowinds inferred from detrital-zircon geochronology of upper Paleozoic loessite, western equatorial Pangea. Geology 30 (8), 695–698. https://doi.org/10.1130/0091-7613(2002)030<0695:PIFDZG>2.0.CO;2.
Soreghan, G.S., Soreghan, M.J., Hamilton, M.A., 2008. Origin and significance of loess in late Paleozoic western Pangaea: a record of tropical cold? Palaeogeogr. Palaeoclimatol. Palaeoecol. 268 (3–4), 234–259. https://doi.org/10.1016/j.palaeo.2008.03.050.
Soreghan, M.J., Heavens, N., Soreghan, G.S., Link, P.K., Hamilton, M.A., 2014. Abrupt and high-magnitude changes in atmospheric circulation recorded in the Permian Maroon Formation, tropical Pangaea. Bulletin 126 (3–4), 569–584. https://doi.org/10.1130/B30840.1.
Stevens, T., Carter, A., Watson, T.P., Vermeesch, P., Andò, S., Bird, A.F., Lu, H., Garzanti, E., Cottam, M.A., Sevastjanova, I., 2013. Genetic linkage between the Yellow River, the Mu Us desert and the Chinese loess plateau. Quat. Sci. Rev. 78, 355–368. https://doi.org/10.1016/j.quascirev.2012.11.032.
Sun, J., 2002. Provenance of loess material and formation of loess deposits on the Chinese Loess Plateau. Earth Planet. Sci. Lett. 203 (3–4), 845–859. https://doi.org/10.1016/S0012-821X(02)00921-4.
Sun, J., 2005. Nd and Sr isotopic variations in Chinese eolian deposits during the past 8 Ma: implications for provenance change. Earth Planet. Sci. Lett. 240 (2), 454–466. https://doi.org/10.1016/j.epsl.2005.09.019.
Sun, J., Windley, B.F., 2015. Onset of aridification by 34 Ma across the Eocene-Oligocene transition in Central Asia. Geology 43 (11), 1015–1018. https://doi.org/10.1130/G37165.1.
Sun, J., Zhu, X., 2010. Temporal variations in Pb isotopes and trace element concentrations within Chinese eolian deposits during the past 8 Ma: implications for provenance change. Earth Planet. Sci. Lett. 290 (3–4), 438–447. https://doi.org/10.1016/j.epsl.2010.01.001.
Sun, D., Liu, D., Chen, M., An, Z., John, S., 1997. Magnetostratigraphy and palaeoclimate of red clay sequences from Chinese Loess Plateau. Sci. China Ser. D Earth Sci. 40 (4), 337–343. https://doi.org/10.1007/BF02877564.
Sun, D., Shaw, J., An, Z., Cheng, M., Yue, L., 1998a. Magnetostratigraphy and paleoclimatic interpretation of a continuous 7.2 Ma Late Cenozoic eolian sediments from the Chinese Loess Plateau. Geophys. Res. Lett. 25 (1), 85–88. https://doi.org/10.1029/97GL03353.
Sun, D., An, Z., Shaw, J., Bloemendal, J., Sun, Y., 1998b. Magnetostratigraphy and palaeoclimatic significance of Late Tertiary aeolian sequences in the Chinese Loess Plateau. Geophys. J. Int. 134 (1), 207–212. https://doi.org/10.1046/j.1365-246x.1998.00553.x.
Sun, J., Zhang, M., Liu, T., 2001. Spatial and temporal characteristics of dust storms in China and its surrounding regions, 1960–1999: relations to source area and climate. J. Geophys. Res. 106 (D10), 10325–10333. https://doi.org/10.1029/2000JD900665.
Sun, D., Bloemendal, J., Rea, D.K., Vandenberghe, J., Jiang, F., An, Z., Su, R., 2002. Grain-size distribution function of polymodal sediments in hydraulic and aeolian environments, and numerical partitioning of the sedimentary components. Sediment. Geol. 152 (3–4), 263–277. https://doi.org/10.1016/S0037-0738(02)00082-9.
Sun, D., Bloemendal, J., Rea, D.K., An, Z., Vandenberghe, J., Lu, H., Su, R., Liu, T., 2004. Bimodal grain-size distribution of Chinese loess, and its palaeoclimatic implications. Catena 55 (3), 325–340. https://doi.org/10.1016/S0341-8162(03)00109-7.
Sun, Y., Lu, H., An, Z., 2006. Grain size of loess, palaeosol and Red Clay deposits on the Chinese Loess Plateau: significance for understanding pedogenic alteration and palaeomonsoon evolution. Palaeogeogr. Palaeoclimatol. Palaeoecol. 241 (1), 129–138. https://doi.org/10.1016/j.palaeo.2006.06.018.
Sun, J., Ye, J., Wu, W., Ni, X., Bi, S., Zhang, Z., Liu, W., Meng, J., 2010. Late Oligocene–Miocene mid-latitude aridification and wind patterns in the Asian interior. Geology 38 (6), 515–518. https://doi.org/10.1130/G30776.1.
Sun, Y., Yan, Y., Nie, J., Li, G., Shi, Z., Qiang, X., Chang, H., An, Z., 2020. Source-to-sink fluctuations of Asian eolian deposits since the late Oligocene. Earth Sci. Rev. 102963 https://doi.org/10.1016/j.earscirev.2019.102963.
Szalai, Z., Király, C., Jakab, G., Szabó, J.A., Varga, G., 2019, January. Application of Raman spectroscopy combined automated 2D image analysis for geosciences. Geophys. Res. Abstr. 21.
Talbot, M.R., Holm, K., Williams, M.A.J., 1994. Sedimentation in low-gradient desert margin systems: a comparison of the Late Triassic of northwest Somerset (England) and the late Quaternary of east-central Australia. Geol. Soc. Am. Spec. Pap. 289, 97–117.
Tsoar, H., Pye, K., 1987. Dust transport and the question of desert loess formation. Sedimentology 34 (1), 139–153. https://doi.org/10.1111/j.1365-3091.1987.tb00566.x.
Újvári, G., Kok, J.F., Varga, G., Kovács, J., 2016. The physics of wind-blown loess: implications for grain size proxy interpretations in Quaternary paleoclimate studies. Earth Sci. Rev. 154, 247–278. https://doi.org/10.1016/j.earscirev.2016.01.006.
van der Does, M., Knippertz, P., Zschenderlein, P., Harrison, R.G., Stuut, J.B.W., 2018. The mysterious long-range transport of giant mineral dust particles. Sci. Adv. 4 (12) https://doi.org/10.1126/sciadv.aau2768 eaau2768.
van Hateren, J.A., Prins, M.A., van Balen, R.T., 2018. On the genetically meaningful decomposition of grain-size distributions: a comparison of different end-member modelling algorithms. Sediment. Geol. 375, 49–71. https://doi.org/10.1016/j.sedgeo.2017.12.003.
van Hateren, J.A., van Buuren, U., Arens, S.M., van Balen, R.T., Prins, M.A., 2019. Identifying sediment transport mechanisms from grain size-shape distributions. Earth Surf. Dynam. Discuss. https://doi.org/10.5194/esurf-2019-58 (in review).
van Toorenenburg, K.A., Donselaar, M.E., Weltje, G.J., 2018. The life cycle of crevasse splays as a key mechanism in the aggradation of alluvial ridges and river avulsion. Earth Surf. Process. Landf. 43 (11), 2409–2420. https://doi.org/10.1002/esp.4404.
Vandenberghe, J., 2013. Grain size of fine-grained windblown sediment: a powerful proxy for process identification. Earth Sci. Rev. 121, 18–30. https://doi.org/10.1016/j.earscirev.2013.03.001.
Vandenberghe, J., Renssen, H., van Huissteden, K., Nugteren, G., Konert, M., Lu, H., Dodonov, A., Buylaert, J.P., 2006. Penetration of Atlantic westerly winds into Central and East Asia. Quat. Sci. Rev. 25 (17–18), 2380–2389. https://doi.org/10.1016/j.quascirev.2006.02.017.
Vandenberghe, J., Sun, Y., Wang, X., Abels, H.A., Liu, X., 2018. Grain-size characterization of reworked fine-grained aeolian deposits. Earth Sci. Rev. 177, 43–52. https://doi.org/10.1016/j.earscirev.2017.11.005.
Varga, G., Kovács, J., Szalai, Z., Cserháti, C., Újvári, G., 2018. Granulometric characterization of paleosols in loess series by automated static image analysis. Sediment. Geol. 370, 1–14. https://doi.org/10.1016/j.sedgeo.2018.04.001.
Varga, G., Gresina, F., Újvári, G., Kovács, J., Szalai, Z., 2019a. On the reliability and comparability of laser diffraction grain size measurements of paleosols in loess records. Sediment. Geol. https://doi.org/10.1016/j.sedgeo.2019.05.011.
Varga, G., Újvári, G., Kovács, J., 2019b. Interpretation of sedimentary (sub) populations extracted from grain size distributions of Central European loess-paleosol series. Quat. Int. 502 (Part A), 60–70. https://doi.org/10.1016/j.quaint.2017.09.021.
Vos, K., Vandenberghe, N., Elsen, J., 2014. Surface textural analysis of quartz grains by scanning electron microscopy (SEM): from sample preparation to environmental interpretation. Earth Sci. Rev. 128, 93–104. https://doi.org/10.1016/j.earscirev.2013.10.013.
Wang, Y.X., Yang, J.D., Chen, J., Zhang, K.J., Rao, W.B., 2007. The Sr and Nd isotopic variations of the Chinese Loess Plateau during the past 7 Ma: Implications for the East Asian winter monsoon and source areas of loess. Palaeogeogr. Palaeoclimatol. Palaeoecol. 249 (3–4), 351–361. https://doi.org/10.1016/j.palaeo.2007.02.010.
Wang, W.T., Zhang, P.Z., Kirby, E., Wang, L.H., Zhang, G.L., Zheng, D.W., Chai, C.Z., 2011. A revised chronology for Tertiary sedimentation in the Sikouzi basin: implications for the tectonic evolution of the northeastern corner of the Tibetan Plateau. Tectonophysics 505 (1–4), 100–114. https://doi.org/10.1016/j.tecto.2011.04.006.
Wang, B., Zheng, H., He, Z., Wang, P., Kaakinen, A., Zhou, X., 2014. Middle Miocene eolian sediments on the southern Chinese Loess Plateau dated by magnetostratigraphy. Palaeogeogr. Palaeoclimatol. Palaeoecol. 411, 257–266. https://doi.org/10.1016/j.palaeo.2014.07.007.
Wang, X., Kraatz, B., Meng, J., Carrapa, B., Decelles, P., Clementz, M., Abdulov, S., Chen, F., 2016a. Central Asian aridification during the late Eocene to early Miocene inferred from preliminary study of shallow marine-eolian sedimentary rocks from northeastern Tajik Basin. Sci. China Earth Sci. 59 (6), 1242–1257. https://doi.org/10.1007/s11430-016-5282-z.
Wang, W., Zhang, P., Liu, C., Zheng, D., Yu, J., Zheng, W., Wang, Y., Zhang, H., Chen, X., 2016b. Pulsed growth of the West Qinling at~ 30 Ma in northeastern Tibet: evidence from Lanzhou Basin magnetostratigraphy and provenance. J. Geophys. Res. 121 (11), 7754–7774. https://doi.org/10.1002/2016JB013279.

Wang, Q., Song, Y., Li, Y., 2019. Clay mineralogy of the upper Miocene-Pliocene red clay from the central Chinese Loess Plateau and its paleoclimate implications. Quat. Int. https://doi.org/10.1016/j.quaint.2019.11.039.

Wasiljeff, J., Kaakinen, A., Salminen, J.M., Zhang, Z., 2020. Magnetostratigraphic constraints on the fossiliferous Ulantatal sequence in Inner Mongolia, China: implications for Asian aridification and faunal turnover before the Eocene-Oligocene boundary. Earth Planet. Sci. Lett. 535, 116125. https://doi.org/10.1016/j.epsl.2020.116125.

Weltje, G.J., Prins, M.A., 2003. Muddled or mixed? Inferring palaeoclimate from size distributions of deep-sea clastics. Sediment. Geol. 162 (1–2), 39–62. https://doi.org/10.1016/S0037-0738(03)00235-5.

Weltje, G.J., Prins, M.A., 2007. Genetically meaningful decomposition of grain-size distributions. Sediment. Geol. 202 (3), 409–424. https://doi.org/10.1016/j.sedgeo.2007.03.007.

Whalley, W.B., Marshall, J.R., Smith, B.J., 1982. Origin of desert loess from some experimental observations. Nature 300 (5891), 433–435.

Wilkins, A.D., Hurst, A., Wilson, M.J., Archer, S., 2018. Palaeo-environment in an ancient low-latitude, arid lacustrine basin with loessite: the Smith Bank Formation (Early Triassic) in the Central North Sea, UK Continental Shelf. Sedimentology 65 (2), 335–359. https://doi.org/10.1111/sed.12382.

Wilson, M.J., Hurst, A., Wilkins, A.D., Wilson, L., Bowen, L., 2020. Mineralogical evidence for multiple dust sources in an early Triassic loessite. Sedimentology 67 (1), 239–260. https://doi.org/10.1111/sed.12641.

Wright, J.S., 2001a. "Desert" loess versus "glacial" loess: quartz silt formation, source areas and sediment pathways in the formation of loess deposits. Geomorphology 36 (3–4), 231–256. https://doi.org/10.1016/S0169-555X(00)00060-X.

Wright, J.S., 2001b. Making loess-sized quartz silt: data from laboratory simulations and implications for sediment transport pathways and the formation of 'desert' loess deposits associated with the Sahara. Quat. Int. 76, 7–19. https://doi.org/10.1016/S1040-6182(00)00085-9.

Wright, J.S., 2007. An overview of the role of weathering in the production of quartz silt. Sediment. Geol. 202 (3), 337–351. https://doi.org/10.1016/j.sedgeo.2007.03.024.

Wright, V.P., Marriott, S.B., 2007. The dangers of taking mud for granted: lessons from Lower Old Red Sandstone dryland river systems of South Wales. Sediment. Geol. 195 (1–2), 91–100. https://doi.org/10.1016/j.sedgeo.2006.03.028.

Wu, L., Krijgsman, W., Liu, J., Li, C., Wang, R., Xiao, W., 2020. CFLab: a MATLAB GUI program for decomposing sediment grain size distribution using Weibull functions. Sediment. Geol. 105590 https://doi.org/10.1016/j.sedgeo.2020.105590.

Xiao, J., Inouchi, Y., Kumai, H., Yoshikawa, S., Kondo, Y., Liu, T., An, Z., 1997. Eolian quartz flux to Lake Biwa, central Japan, over the past 145,000 years. Quat. Res. 48 (1), 48–57. https://doi.org/10.1006/qres.1997.1893.

Xu, Y., Yue, L., Li, J., Sun, L., Sun, B., Zhang, J., Ma, J., Wang, J., 2009. An 11-Ma-old red clay sequence on the Eastern Chinese Loess Plateau. Palaeogeogr. Palaeoclimatol. Palaeoecol. 284 (3–4), 383–391. https://doi.org/10.1016/j.palaeo.2009.10.023.

Xu, Y., Li, J., Pan, F., Yang, B., Tang, Y., Bi, Y., Li, T., Yue, L., Wingate, M.T., 2018. Late Neogene aridification and wind patterns in the Asian interior: Insight from the grain-size of eolian deposits in Altun Shan, northern Tibetan Plateau. Palaeogeogr. Palaeoclimatol. Palaeoecol. 511, 532–540. https://doi.org/10.1016/j.palaeo.2018.09.017.

Yan, Y., Ma, L., Sun, Y., 2017. Tectonic and climatic controls on provenance changes of fine-grained dust on the Chinese Loess Plateau since the late Oligocene. Geochim. Cosmochim. Acta 200, 110–122. https://doi.org/10.1016/j.gca.2016.12.009.

Yang, S.L., Ding, Z.L., 2004. Comparison of particle size characteristics of the Tertiary 'red clay' and Pleistocene loess in the Chinese Loess Plateau: implications for origin and sources of the 'red clay'. Sedimentology 51 (1), 77–93. https://doi.org/10.1046/j.1365-3091.2003.00612.x.

Yang, S., Ding, Z., 2010. Drastic climatic shift at~ 2.8 Ma as recorded in eolian deposits of China and its implications for redefining the Pliocene-Pleistocene boundary. Quat. Int. 219 (1–2), 37–44. https://doi.org/10.1016/j.quaint.2009.10.029.

Zachos, J.C., Dickens, G.R., Zeebe, R.E., 2008. An early Cenozoic perspective on greenhouse warming and carbon-cycle dynamics. Nature 451 (7176), 279–283. https://doi.org/10.1038/nature06588.

Zhang, J., Li, J., Song, C., Zhao, Z., Xie, G., Wang, X., Hui, Z., Peng, T., 2013. Paleomagnetic ages of Miocene fluvio-lacustrine sediments in the Tianshui Basin, western China. J. Asian Earth Sci. 62, 341–348. https://doi.org/10.1016/j.jseaes.2012.10.014.

Zhang, Y., Sun, D., Li, Z., Wang, F., Wang, X., Li, B., Guo, F., Wu, S., 2014. Cenozoic record of aeolian sediment accumulation and aridification from Lanzhou, China, driven by Tibetan Plateau uplift and global climate. Glob. Planet. Chang. 120, 1–15. https://doi.org/10.1016/j.gloplacha.2014.05.009.

Zhang, H., Lu, H., Stevens, T., Feng, H., Fu, Y., Geng, J., Wang, H., 2018. Expansion of dust provenance and aridification of Asia since~ 7.2 Ma revealed by detrital zircon U-Pb dating. Geophys. Res. Lett. 45 (24), 13–437. https://doi.org/10.1029/2018GL079888.

Zheng, H., 2016. Asia dust production ramped up since latest Oligocene driven by Tibetan Plateau uplift. Natl. Sci. Rev. 3 (3), 271–274. https://doi.org/10.1093/nsr/nww028.

Zheng, H., An, Z., Shaw, J., 1992. New contributions to Chinese Plio-pleistocene magnetostratigraphy. Phys. Earth Planet. Inter. 70 (3–4), 146–153. https://doi.org/10.1016/0031-9201(92)90177-W.

Zheng, H., Wei, X., Tada, R., Clift, P.D., Wang, B., Jourdan, F., Wang, P., He, M., 2015. Late oligocene–early miocene birth of the Taklimakan Desert. Proc. Natl. Acad. Sci. 112 (25), 7662–7667. https://doi.org/10.1073/pnas.1424487112.

Zhou, L.P., Oldfield, F., Wintle, A.G., Robinson, S.G., Wang, J.T., 1990. Partly pedogenic origin of magnetic variations in Chinese loess. Nature 346 (6286), 737–739. https://doi.org/10.1038/346737a0.

Zhu, Y., Zhou, L., Mo, D., Kaakinen, A., Zhang, Z., Fortelius, M., 2008. A new magnetostratigraphic framework for late Neogene Hipparion Red Clay in the eastern Loess Plateau of China. Palaeogeogr. Palaeoclimatol. Palaeoecol. 268 (1–2), 47–57. https://doi.org/10.1016/j.palaeo.2008.08.001.